UiT
THE ARCTIC
UNIVERSITY
OF NORWAY

Faculty of Science and Technology
Department of Physics and Technology

# Renewable Energy Resources:

*A Case Study on Asko Nord AS*

—

**Sondre Solstad**

*EOM-3901 Master thesis in energy, climate and environment - June 2016*

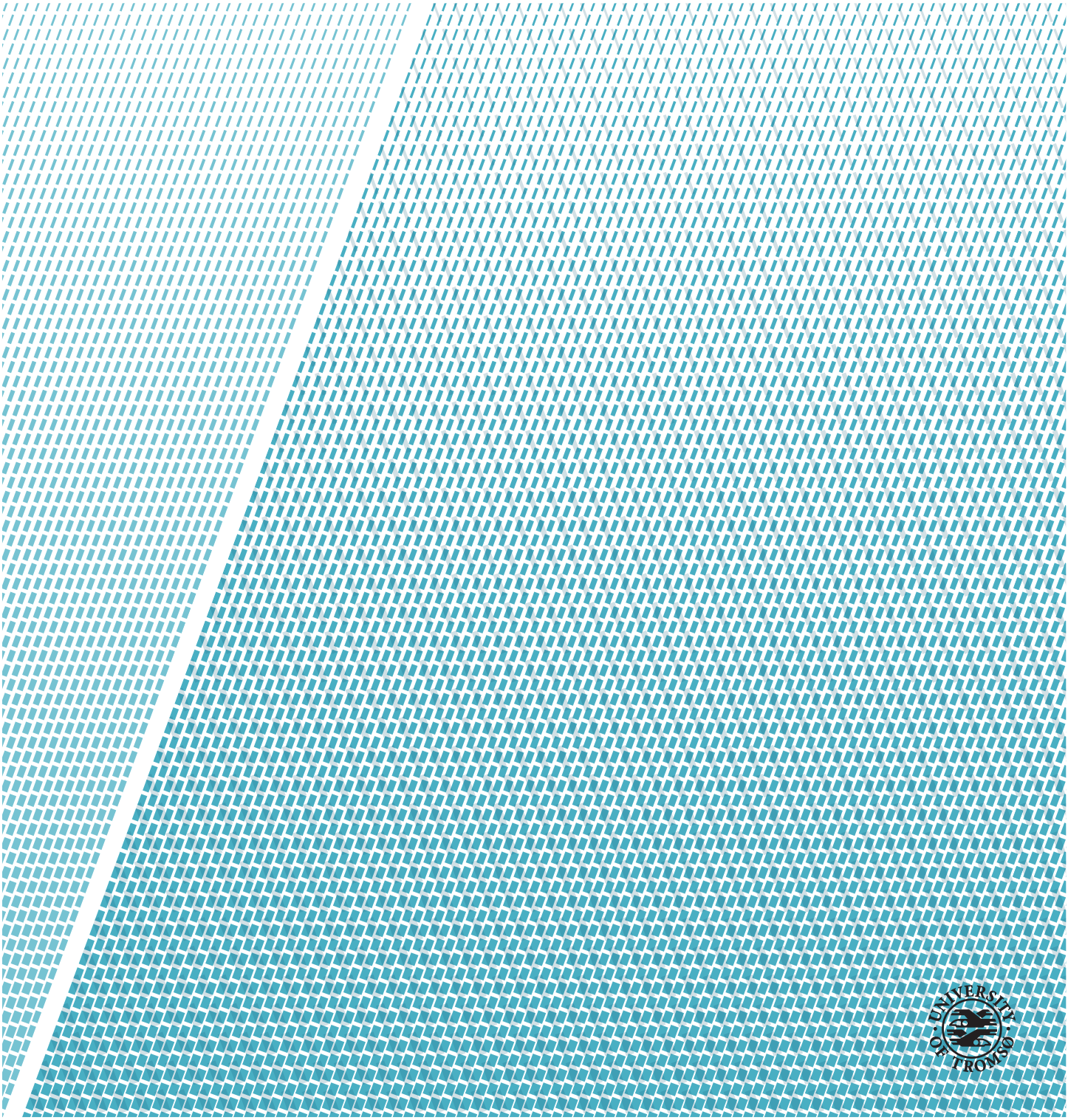

# Abstract

Asko Nord AS i a business located in Ramfjorden just outside of Tromsø. In this theses, their potential to produce electricity from renewable resources at their location is investigated. Wind around the building is to find suitable locations for wind turbines, and to estimate the wind at the wind turbines. The calculations show that in a feasible estimate the wind is able to produce 439 $kwh$ from each square meter the wind turbine sweeps. Solar measurement and local conditions are used to calculate optimal orientation and tilt of the solar panels. The results show that with optimal tilting, solar panels are able to produce 166 $kwh$ per square meter of solar panels and even more if the panels are tracking the sun's motion. The theses ends with a example where solar panels and wind turbines are selected. This shows that Asko, in this case, is able to produce 9.8% of its usage.

# Acknowledgements

Jeg vil gjerne takke min veileder Tobias Boström for åpen dør og nyttige tilbakemeldinger.

Jeg vil takke Asko Nord AS ved Arne Sørensen, Rune Larsen og Grete Ovanger for å gi meg tilgang til verdifull informasjon og data å jobbe med. Håper oppgaven kan være et hjelpemiddel i fremtiden for gode invsteringer i fornybar energi.

Jeg må takke mine medstudenter på energi, klima og miljø for fem interessante år, samt andre studenter jeg har blitt godt kjent med gjennom studietiden.

Jeg vil takke Ellen Sørgård for omfattende korrekturlesing.

Sist men ikke mist må familie og venner takkes for støtte, mat og oppmuntring gjennom alle årene, spesielt det siste semesteret.

# Nomenclature

| | | |
|---|---|---|
| $E_k$ | kinetic energy | [J] |
| $\boldsymbol{F}$ | force | [N] |
| P | power | [W] |
| v | speed | [m/s] |
| $\boldsymbol{v}$ | velocity | [m/s] |
| m | mass | [kg] |
| $\rho$ | density | [kg/m$^3$] |
| p | pressure | [Pa] |
| $\nu$ | kinetic viscosity | [Ps s] |
| $n_i$ | intrinsic carrier concentration | [1] |
| K | kelvin | [1] |
| el | elevation | [ °] |
| az | azimuth | [ °] |

# Abbreviations

**CFD** Computational fluid dynamics

**LES** Large-eddy simulation

**HAWT** Horizontal-axis wind turbine

**VAWT** Vertical-axis wind turbine

**STC** Standard test condition

**Si** Silicon

**P** Phosphorus

**AM** Air mass

**HRA** Hour angle

**LST** Local solar time

**TC** Time correction factor

**EoT** Equation of time

**LSTM** Local standard time meridian

**mph** miles per hour

**MWS** measured wind speed

**WS10** Wind speed at 10 meter

# Contents

# List of Figures

# List of Tables

# 1 Introduction

The world energy demand is increasing. According to BP, the global energy consumption have increased on average 2.1 % the last ten years. In 2014, only 3.0 % of the energy consumption was from renewable resources[13]. The world is challenged with global climate change. The usage of fossil fuel and emittance of $CO_2$ contribute to the change[31].

With the world energy demand growing and the need to stop global climate change, changes from fossil energy towards renewable is necessary. It is not only environmental reasons for the need of change towards renewable. The proven oil resources were, 1700 thousand million barrels in 2014. The daily usage the same year was 92'086 thousand barrels[13]. With this usage, the proven resources will last 50 years. More oil will be found. However, as the known resources are getting smaller, the price will eventually increase. The resources available from solar and wind are estimated by C.L. Archer [5] and shown in figure 1.1. This illustrates that renewable resources are capable of handling the future energy demand.

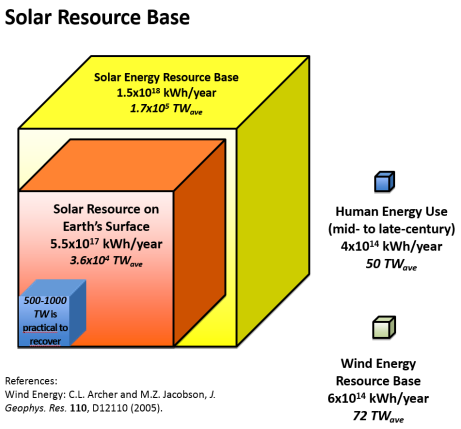


**Figure 1.1:** Estimate of solar and wind resources [5].

Likewise, there is a common thinking that you are only a small part of the change and your work will not make the difference. However, to succeed with the goals set to reduce fossil energy usage the changes need to be made locally as well as globally.

## 1.1 Aim of study

Asko Nord AS, hereafter referred to as Asko, want to contribute to the change towards more renewable energy. The investment is potentially high, therefore a pre-study is necessary before investing. This theses is a pre-study for Asko and their building in Ramfjorden outside Tromsø, Norway. The goal of the pre-study is to determine the amount of electricity Asko is able to produce from solar and wind resources.

## 1.2 Structure of the study

The study has two focus parts, solar and wind, and most chapters are split between them There are five chapters: introduction, theory, method, results with discussion, and conclusion. Chapter one gives the necessary introduction to the theory needed to make decisions and calculate the theoretical energy production. It explains techniques and equations needed in the method chapter.

The method is the binding between the theory and the results. Here, the overview of the wind simulation program and the variables are discussed. The process of calculating the energy at the specific site is explained with the local information needed.

The results chapter starts with a representation of untreated data and follows the evolution as the methods is used and the raw data is transformed to amount of electricity. In the end, an example for Asko is created.

The conclusion summarizes the thesis and note important parts.

# 2 Theory

The theory is divided between wind and solar. Where both sections goes from the origin of the renewable energy source to production of electricity from it.

## 2.1 Wind

### 2.1.1 Source of wind

Wind is formed from pressure differences. If one area has high pressure and another has low, the air will flow from the high pressure to the low pressure in search for equilibrium. Pressure is dependent on temperature. At low temperatures, the air is more dense. The denser air flows toward the uncompressed air at warm areas. Figure 2.1 shows that the concentration of the sun's radiation is higher near the equator and lower closer to the poles. This will produce a low pressure around the equator and a higher pressure towards the poles. Wind goes towards the equator at ground level, the heat at equator makes the air rise, the stratosphere will work as a lid

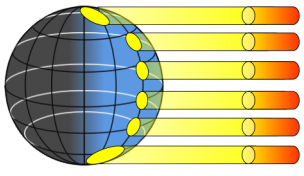

**Figure 2.1:** Solar incidence on Earth

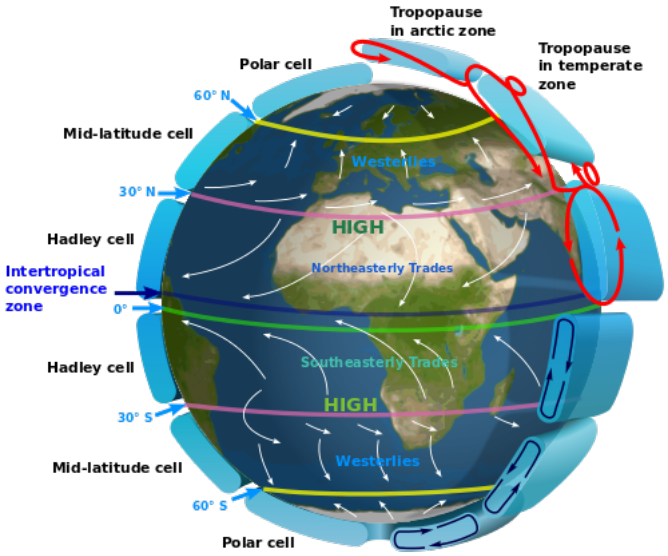


**Figure 2.2:** Wind cells on Earth. Figure from [19]

making the air move towards the poles high up. As the air moves higher it gets cooler, and at about 30 degrees north it sinks, making a cell known as a hadley cell, [2]. See figure 2.2[19]. The sinking air at 30 degree north does not only flow towards the equator, but also the poles. This produces a second cell, the mid-latitude cell from 30 degree north to 60 degree north. The last cell, named polar cell, bring cold air from the poles towards the low pressure area at 60 degree north. The corresponding cells in produced at the souther hemisphere.

The phenomenon described above is the background for wind movement north or south. The earth rotation and Coriolis force will give a bending towards the right in the velocity direction in the northern hemisphere and left to the velocity direction in the southern hemisphere. This is not enough to predict wind behaviour. The cells are not permanent at one place all the time. Seasonal changes and other weather related fluctuations will always change the cells. Land, mountains and fjords contribute to wind directions. Local weather causes local high and low pressure areas that will give local winds.

### 2.1.2 Wind distribution

Wind speed is not steady, therefore a statistical presentation is used.

### Weibull distribution

Weibull distributions are commonly used to represent wind speed[36]. When wind speed is Weibull distributed, the density function is as follows [6]

$$f(x;a,b) = \frac{b}{a}\left(\frac{x}{a}\right)^{b-1} e^{-(\frac{x}{a})^b} \ , x \geq 0 \tag{2.1.1}$$

The cumulative distribution function is as follows [6]

$$F(x;a,b) = 1 - e^{-(\frac{x}{a})^b} \ , x \geq 0 \tag{2.1.2}$$

The shape of the density function and the cumulative distribution are dependent of $a$ and $b$. $a$ have the same dimension as $x$, often meters per second and $b$ is dimensionless[7]. $b$ determines the shape and $a$ determines the scale. Figure 2.3a shows how the shapes change. If $b$ is below one, the shape will be similar to an exponential function, and if $b$ is above one, the shape will be more like an rayleigh distribution. Figure 2.3b shows how the same shape is stretched outwards when a is changing.

### Maximum likelihood method

The parameters $a$ and $b$ have to be determined. One way to determine them is with the maximum likelihood method[36].

$$b = \left(\frac{\sum_{i=1}^{n} v_i^b ln(v_i)}{\sum_{i=1}^{n} v_i^b} - \frac{\sum_{i=1}^{n} ln(v_i)}{n}\right)^{-1} \tag{2.1.3}$$

$$a = \left(\frac{1}{n}\sum_{i=1}^{n} v_i^b\right)^{\frac{1}{b}} \tag{2.1.4}$$

This method is possible to use when a set of wind measurements is available. $v_i$ is the wind speed at sample i and n is the total number samples of the set. Equation (2.1.3) needs to be solved with iterations. When $b$ is determined, equation (2.1.4) will give $a$.

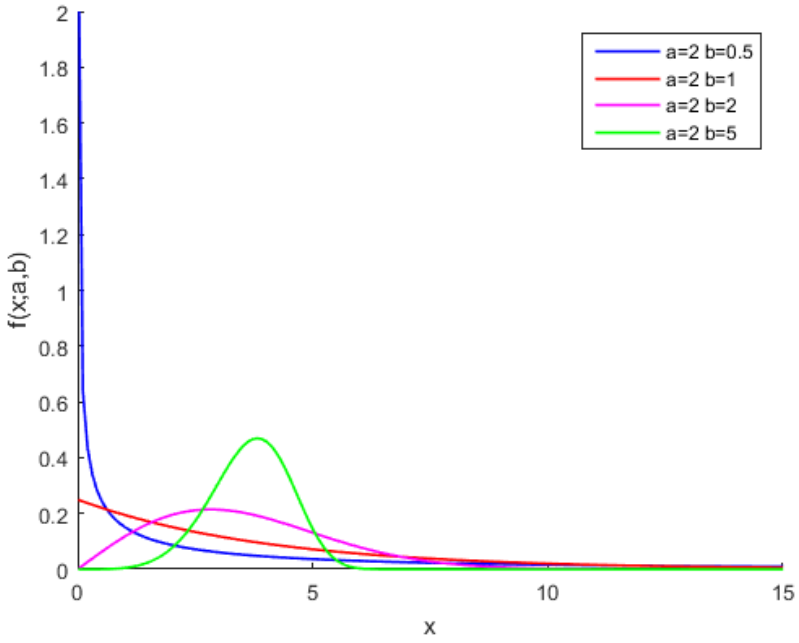


**(a)** Constant a and changing b values

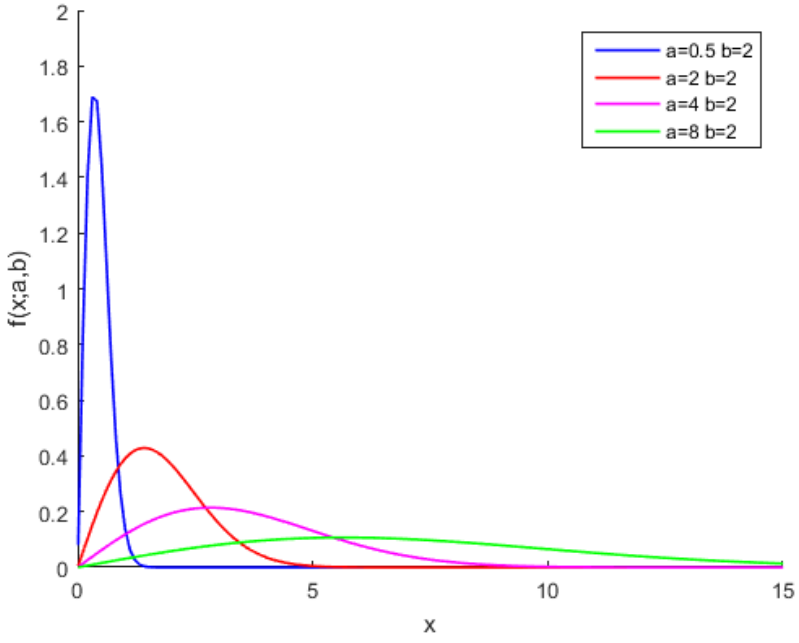


**(b)** Constant b and changing a values

**Figure 2.3:** Weibull distrubution

### 2.1.3 Power in wind

The total kinetic energy of any moving object with a mass m and speed v is:

$$KE = \frac{1}{2} m \cdot v^2 \tag{2.1.5}$$

From this the power is the energy divided by time t:

$$P = \frac{KE}{t} = \frac{1}{2} \frac{m \cdot v^2}{t} \tag{2.1.6}$$

The density $\rho$ is defined as:

$$\begin{aligned} \rho &= \frac{m}{V} \\ m &= \rho \cdot V \\ m &= \rho \cdot A \cdot L \\ m &= \rho \cdot A \cdot v \cdot t \end{aligned} \tag{2.1.7}$$

V is volume, A is the area the wind turbine sweeps and L is length. The combination of equation (2.1.6) and equation (2.1.7) will give the power in wind as a function of the wind speed $v$, density of the air $\rho_{air}$ and area A.

$$P = \frac{1}{2} * \rho * v^3 * A \tag{2.1.8}$$

This equation is all based on [28]. From equation 2.1.8 it is important to note that the power increases with third power of the wind speed $v$.

### 2.1.4 Horizontal wind shear

Depending on many factors, the wind speed will change moving from the ground and upwards. The power law for wind shear[28] is a general method for estimating the wind speed at different heights based on wind speed at a known height.

$$v = v_0 \left( \frac{H}{H_0} \right)^{\alpha} \tag{2.1.9}$$

$v$ is the unknown wind speed, $v_0$ is measured wind speed, H is the height of $v$, $H_0$ is the height of $v_0$ and $\alpha$ is the wind shear exponent. The wind shear exponent depends on atmosphere and ground conditions. Kaltschmitt et al. [20] made a table of approximation of the share exponent with values differing from 0.06 to 0.60. The table is copied in table 2.1. Nelson [28] operates with $\alpha = 0.14$, which describes a stable atmosphere. However, the best way to determine the wind share exponent is to calculate it from measurements at different heights.

| Stability | Open water surface | Flat, open coast | Cities, villages |
|---|---|---|---|
| Unstable | 0.06 | 0.11 | 0.27 |
| Neutral | 0.10 | 0.16 | 0.34 |
| Stable | 0.27 | 0.40 | 0.60 |

**Table 2.1:** Approximation of different wind shear exponents under different conditions. Table from [20]

**(a)** Horizontal-axis wind turbine. Photo from [22].

**(b)** Vertical-axis wind turbine. Photo from [44].

**Figure 2.4:** example of HAWT and VAWT

### 2.1.5 Wind turbines

Wind turbines convert the kinetic energy in wind to electricity. There are different types of wind turbines. Common for most of them are that blades get rotational speed from the wind. The rotational speed goes directly to a generator or through a gear before the generator. There are two main types of wind turbine, horizontal-axis wind turbines (HAWT) and vertical-axis wind turbines (VAWT).

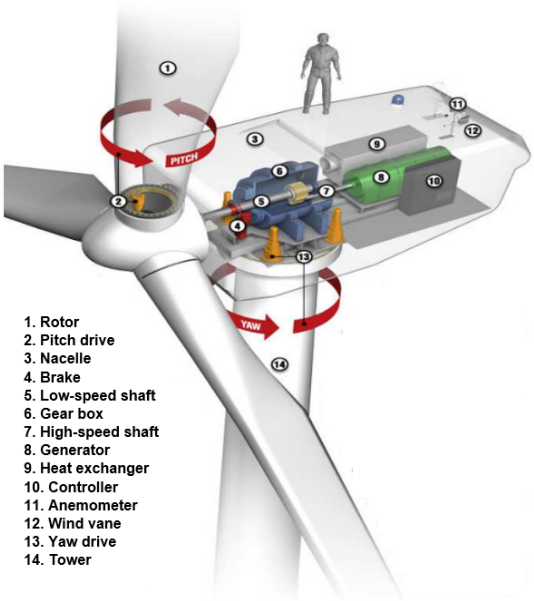


**Figure 2.5:** Model of HAWT. Figure from Schubel and Crossley [35] and modified by Jacobsen [17]

### Horizontal-axis wind turbine

HAWT is the section of wind turbines that rotate at a horizontal level according to figure 2.4a. Most HAWTs have a nacelle with gearbox, generator and other components on top of a tower according figure 2.5.

### Vertical-axis wind turbine

VAWT rotate around a vertical axis. There are different types of VAWT. The most common are Darrieus, H-type(giromill) and Savonius.

A Savonius turbine is illustrated to the left in figure 2.6. It is one of the simplest turbines, having two or more scopes. On a Savonius turbine with two blades the blades will form the shape of an S. The blade facing the wind with an open side will have more drag force than the closed side. The difference in force from the drag at different sides of the vertical axis will make it rotate[35]. There will always be a blade moving opposite to the wind, slowing the rotation of the turbine. Therefore, the Savonuis turbine efficiency will be limited. The benefits

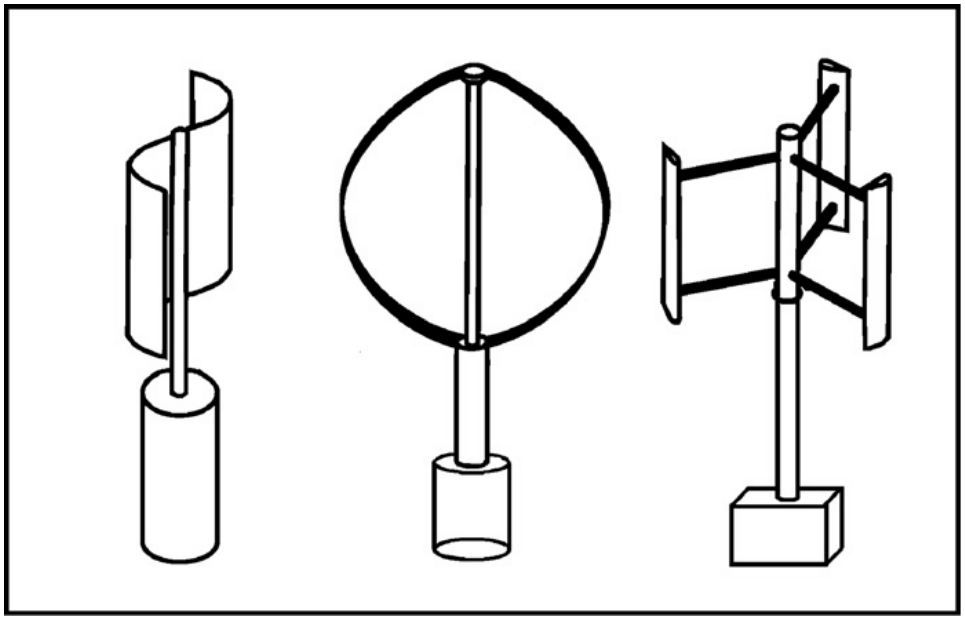

**Figure 2.6:** Savonius to the left, Darrieus in the middel and H-rotor to the right. Illustration from [11]

with Savonuis is that it is self starting and has a very simple construction[42]. There have been done tests on a twisted Savonuis turbine that have higher efficiency at the cost of a more complex structure.

H-rotor or giromill and Darrieus turbines work quite similarly, with blades formed as airfoil. Unlike Savonuis, H-rotor and Darrieus use mostly lift and less drag. The airfoils use wind combined with an initial rotation to produce a pressure difference. The force from the pressure difference increases the rotational speed. Since this wind turbine does not have drag when the blades are facing the wind it has better efficiency. The difference between H-rotor and the Darrieus is the shape of the blades. The Darrieus turbine is in the middle with an egg formed shape and H-rotor, to the right in figure 2.6,has straight blades at a distance from the rotation axis.

The heavy components of the VAWT are, as opposed to HAWT, placed on the ground. This makes it easier to access for maintenance. The main advantage is that the VAWT works with wind from all directions without the need of yaw mechanisms. In areas where the wind circulates or are turbulent, VAWT use the principle of superposition. VAWT can use the wind from all directions, on opposite to HAWT, and will experiences less production and higher risk of damage[42]. There are different opinions about the efficiency of VAWT. A few papers indicate that VAWT have the theoretical potential to exceed the Betz limit[29]. On the other hand, most papers conclude that VAWT have lower

| | H-rotor | Darrieus | HAWT |
|---|---|---|---|
| Blade profile | Simple | Complicated | Complicated |
| Yaw mechanism needed | No | No | Yes |
| Pitch mechanism possible | Yes | No | Yes |
| Tower | Yes | No | Yes |
| Guy wires | Optional | Yes | No |
| Noise | Low | Moderate | High |
| Blade area | Moderate | Large | Small |
| Generator position | On ground | On ground | On top of tower |
| Blade load | Moderate | Low | High |
| Self-starting | No | No | Yes |
| Tower interference | Small | Small | Large |
| Foundation | Moderate | Simple | Extensive |
| Overall structure | Simple | Simple | Complicated |

**Table 2.2:** Difference between H-rotor, Darrieus and HAWT[11]

efficiency than HAWT[32][28][18] and that this is the main disadvantage for VAWT. S. Eriksson et al.[11] have made table 2.2 as an summary between H-rotor, Darrieus and HAWT.

### Coefficient of power and power curve

The only way to use all of the power in wind is to stop it, which is not realistic. Every wind turbine, both VAWT and HAWT, will have a coefficient of power $c_p$ defined as [4]

$$c_p = \frac{P_{Out}}{P_{In}} \tag{2.1.10}$$

Where $P_{Out}$ is the power from the generator and $P_{In}$ is the power in the wind. $c_p$ is limited by the Betz limit which state that no wind turbine is able to convert more than 16/27 or 59.3 %of the potential power in the wind[2]. Jamieson, 2011 [18] suggested a realistic $c_p$ to be 0.50 for HAWT and 0.40 for Darius and H-rotor. The size of the wind turbine is given as rated or nominal power. This is the effect under maximal production. Figure 2.7 shows an example of the power curve for a 1.5 MW wind turbine. This wind turbine does not produce energy at wind speeds lower than 3 $m/s$. This is called the cut-in speed. The production follows the wind speed until the production reaches the nominal power. The wind speed at this point is called the rated wind speed, which at the 1.5 MW exmple is 15 $m/s$. The production is at the nominal power until the cut-out speed at 25 $m/s$ ,where the wind turbine stops to avoid damage.

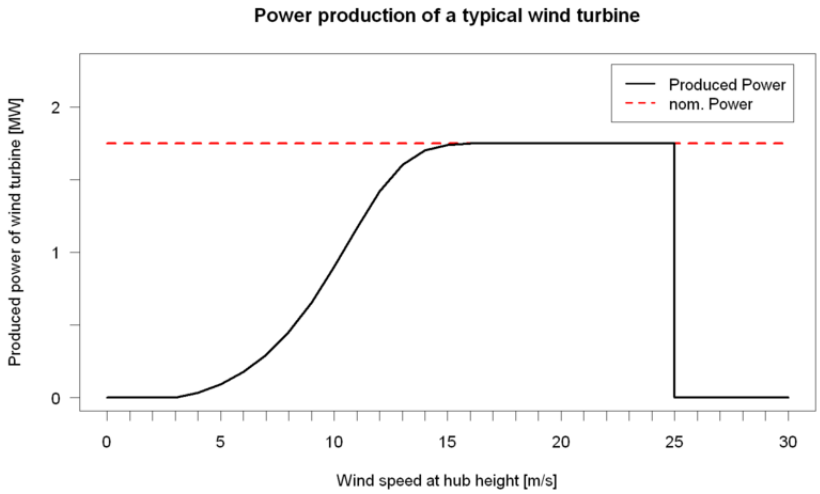


**Figure 2.7:** Powercurve of a typical wind turbine

### 2.1.6 Governing equations in fluid dynamics

The motion of an incompressible fluid is described by Navier-Stokes equations. Equations 2.1.11, 2.1.12 and 2.1.13 are based on Vallis [43] and are derived from these three established equations [1]:

- Mass is conserved
- Newton's second law. Force = mass * acceleration
- Energy is conserved

$$\frac{d\boldsymbol{v}}{dt} = -\frac{\nabla p}{\rho} + \nu\nabla^2\boldsymbol{v} + \boldsymbol{F} \tag{2.1.11}$$

$\boldsymbol{v}$ is the velocity of the fluid, $\rho$ is the density, p is the pressure and $\nu$ is the kinematic viscosity. $\boldsymbol{F}$ is forces affecting the fluid, such as Coriolis and gravity. The mass continuity equation is given as

$$\frac{\partial\rho}{\partial t} + \nabla(\rho\boldsymbol{v}) = 0 \tag{2.1.12}$$

If the density $\rho$ is constant, the continuity equation(2.1.12) will be reduced

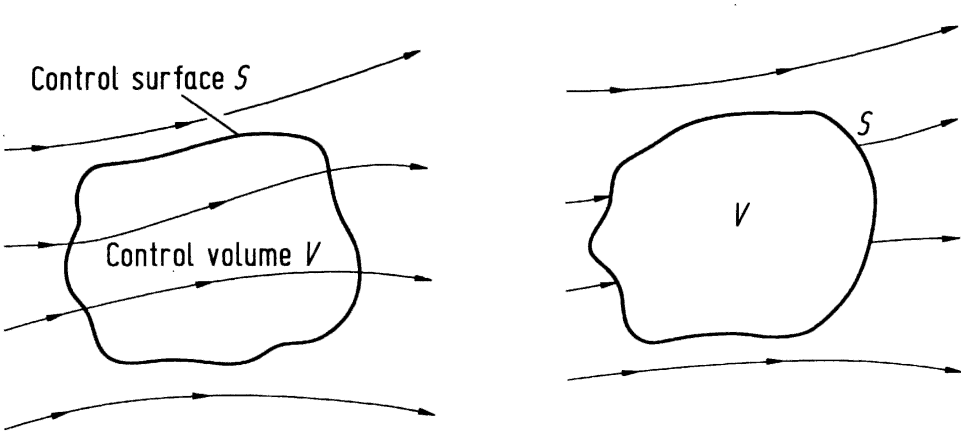


**Figure 2.8:** Finite volume method. Figure from [1]

to

$$\nabla \boldsymbol{v} = 0 \tag{2.1.13}$$

Navier-Stokes equations are difficult to solve. Instead, a method is developed called computational fluid dynamics (CFD). CFD uses computers to solve the equations numerically. There are multiple methods of discretization of Navier-Stokes equations. One of these methods is the finite volume method.

### The finite volume method

The finite volume method is a method where the calculations are done on a specified volume. The volume can be fixed in space as shown on the left side of figure 2.8 or move with the fluid as shown on the right side of figure 2.8. The method discretizes the integral form of the equation and not the differential form [1].

### The turbulence model

In addiction to discretization, turbulence needs to be solved. Direct numerical simulation (DNS), Reynolds-average Navier-Stokes (RANS) and Large-Eddy simulation (LES) are commonly used techniques[23]. DNS solves all scales of turbulence. Due to limitations in computers, LES only calculates the most important scales and approximate the rest. This is done by spatially filtering the equations. The filter is a low pass filter that removes all scale under the cut

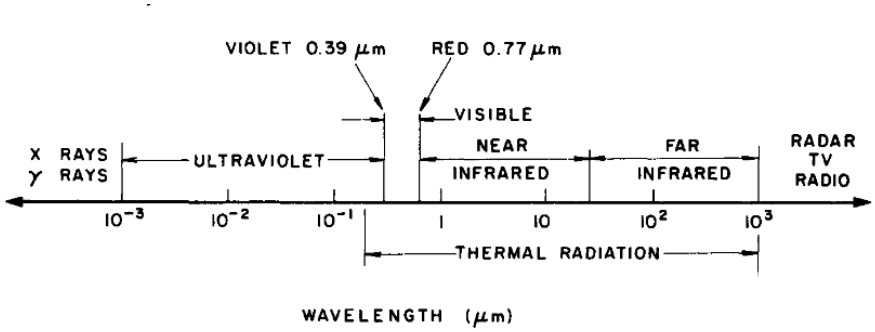


**Figure 2.9:** Spectrum of electromagnetic irradiation. Figure from Iqbal 1983 [16]

off scale.

## 2.2 Solar

### 2.2.1 Properties of sunlight

Electromagnetic radiation consists of different types of waves with wavelengths according to figure 2.9. The wave energy is given by [27]:

$$E = \frac{h * c}{\lambda} \tag{2.2.1}$$

E is the energy, h is Planck's constant, c is the speed of light and $\lambda$ is the wavelength.
A black body is a surface that emits the maximal amount of energy at all wavelengths and absorbs all incident radiation at a given temperature [7]. The sun has a temperature of 5777 K [10] The black body energy spectre of a surface with a temperature of 5777 K is given in the green line of figure 2.10. The red line is the intensity of light from the sun outside our atmosphere, $AM = 0$. The blue line is light intensity at $AM = 1.5$. AM stands for air mass and is the distance the light passes through the atmosphere compared to the shortest way. The shortest way is when the sun is directly above and is equal to $AM = 1$.

### 2.2.2 Solar cells

#### Semiconductors

Materials can be divided into tree groups: insulators, metals and semiconductors. In an insulator, all the electrons are in tight bounds and are not able to

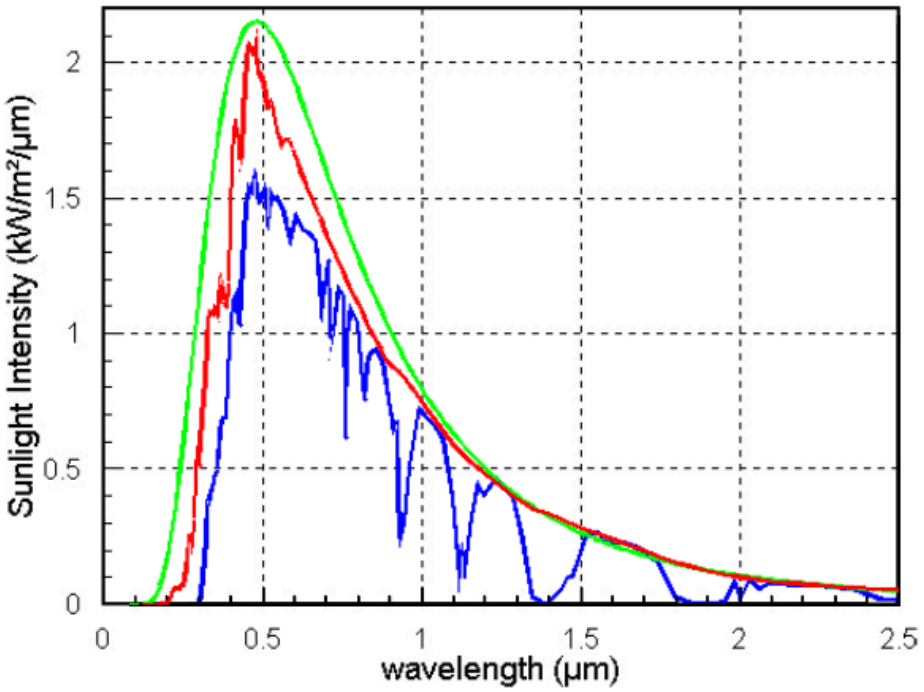


**Figure 2.10:** Illustration of sunlight intensity and wavelength. Figure from Honsberg and Bowden [15].

move freely. In metals, the electrons are able to move freely around and conduct electricity. Semiconductors have characteristics between insulator and metal. In an semiconductor, the electrons are in bounds as an insulator at absolute zero. If the temperature rises, the kinetic energy is enough to break some of the bounds and the electron becomes free, leaving a hole where the electron previously was. This is a electron-hole pair. One of the surrounding electrons in the bounds is free to move into the empty hole, leaving behind another hole. The hole can be illustrated as a positive charged particle through the crystal structure. Both the electron and the hole can conduct current and are often called intrinsic carriers[15]. The number of intrinsic carriers for Si is given as a function of temperature[26].

$$n_i(T) = 5.29 * 10^{19}(\frac{T}{300})^{2.54} * exp(\frac{-6726}{T}) \tag{2.2.2}$$

In the periodic table, semiconductors are either placed in group IV, a combination of III and V or a combination of II and VI. [15]. The most used semiconductor material are silicon (Si). Si atoms will form four covalent bounds with other Si atoms, making a solid structure where every atom has eight electrons in the other bond, similar to figure 2.11.

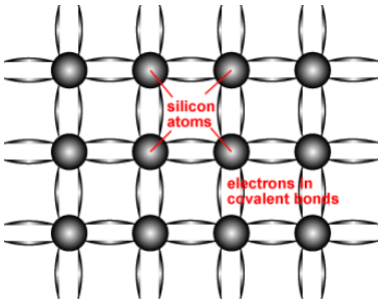


**Figure 2.11:** Covalent bond between Si atoms. Figure from PVeducation [15]

Doping is a method to prevent recombination of the electron-hole pair by creating an electric field inside the semiconductor material. There are two types of doping, n type doping and p type doping.
In n type, some of the atoms are replaced with donor atoms with more electrons then needed to make the covalent bound. Phosphorus (P) in group V has five valence electrons. Only four are needed to make the bounds with the surrounding atoms. Therefore, one of the electrons are not as bound to the structure and can easily become free to move. P type doping works in a similar way, except here the acceptor atom will have less electrons than needed in the valence bound, leaving a hole free to move. Now the atom is called acceptor. Acceptor atoms are from group III in the periodic table[27]. Both donor and acceptor atoms have a neutral charge when used to dope the semiconductor. Therefore, the doped area does not have a positive or negative charge initially. When they are joined, some free electrons and free holes near the junction recombine. When an electron leaves the n-doped side, the net charge becomes

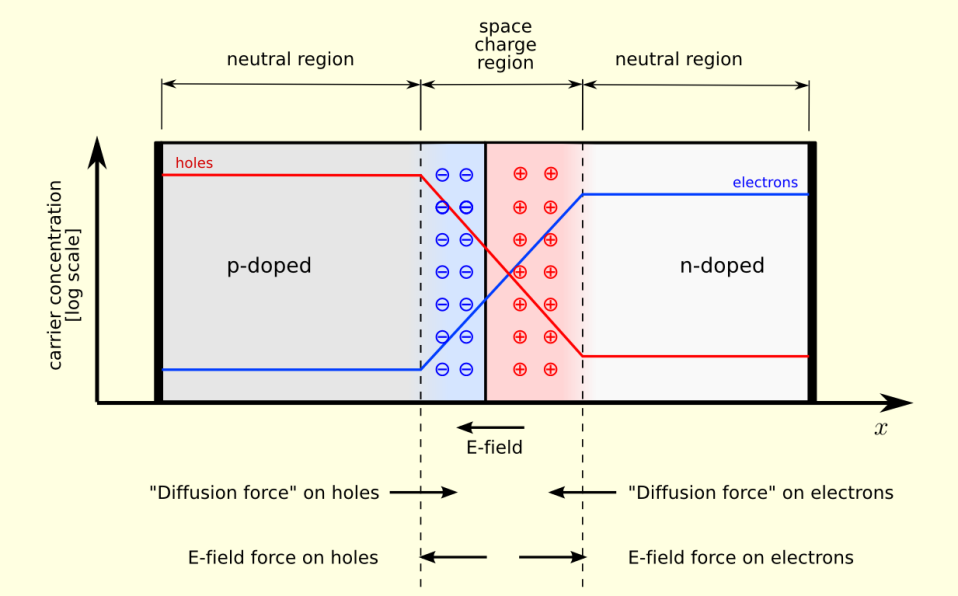


**Figure 2.12:** pn Junction under zero-bias. Figure from [41]

positive, and when a hole leaves the p-doped side, the net charge becomes negative, as shown on figure 2.12. The difference in charge produces an electric field. The electric field area is called the space charge region. A solar cell consists of a semiconductor with pn-junction, covered with an antireflection coating on top, and front and back contacts as figure 2.13 shows. The top part of the semiconductor are called emitter and the bottom is called base. The back contact normally covers the entire back. The front contact consists of busbars and fingers that conduct current with as little shadowing as possible [40]. The solar cell produces electricity by using the energy in the solar waves to create an electron hole pair. The electric field separates the electron from hole. The hole goes through the junction and the electron moves in the external circuit as electricity before they recombine at the same side of the junction.

### 2.2.3 Efficiency and losses

It is not possible to use all of the energy in the solar light to produce electricity. Figure 2.14 is an overview of losses in a typical solar cell due to technological limitations.

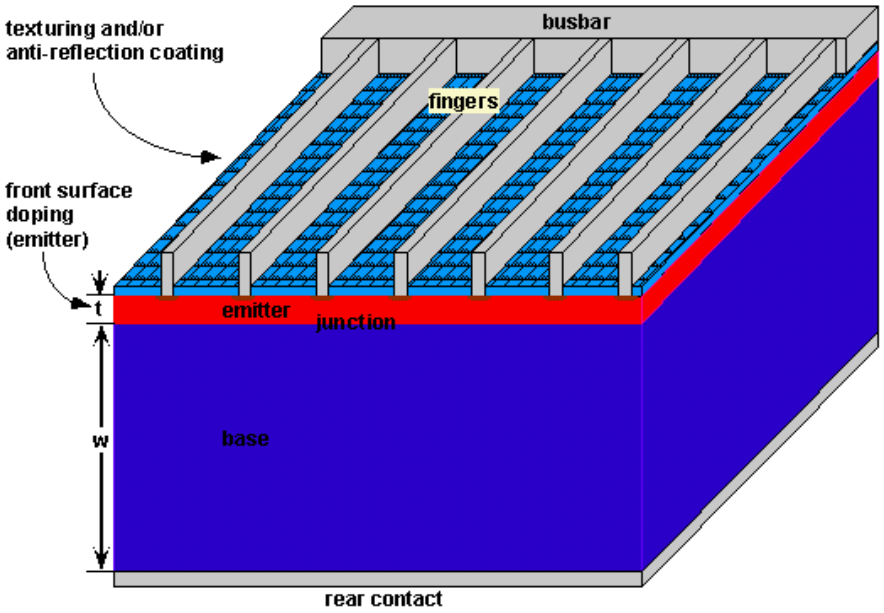


**Figure 2.13:** Illustration of a typical semiconductor solar cell. Figure from PVEducation[15]

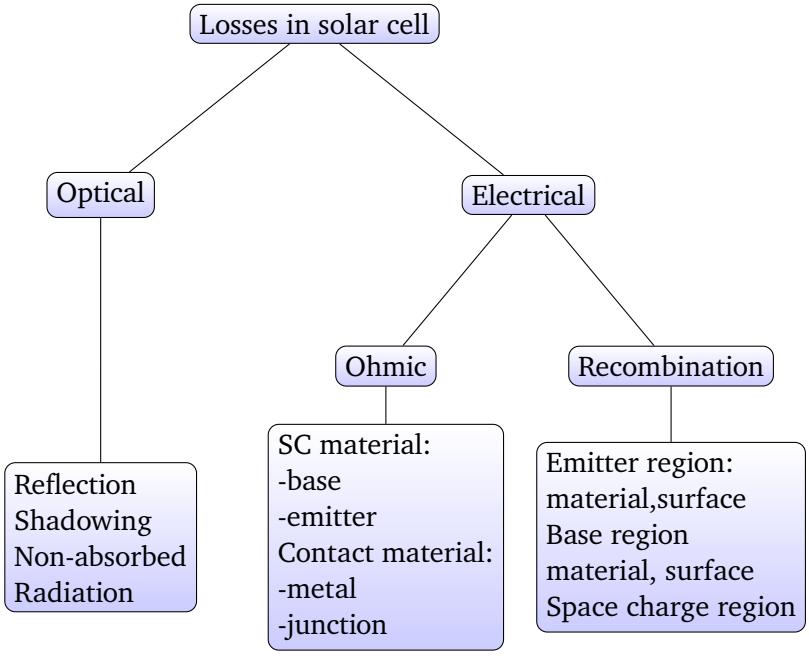


**Figure 2.14:** Losses in solar cell. Figure from Solanki 2011 [38]

### Optical Losses

For the solar cell to be able to produce, the waves need to go into the solar cell. The reflection of Si alone is over 30 % [15]. With techniques such as anti-reflection layers and surface texture, the reflection is reduced. On the surface, the busbars and fingers will shadow small, but significant parts of the solar cell. Calculations have shown that the front contact shadowing is between 3.5 % and 4.5 % depending on the finger spacing [40].

If a photon that gets absorbed in the solar cell have higher energy than needed to create the electron hole pair, the extra energy is lost as heat when the electron thermilize down to the band gap energy level. Solar cells are often thin to save material expenses. Some photons have too much energy to be absorbed by the thin solar cell and contribute to losses as non-absorbed energy.

### Electrical

Electricity is conducted through the different components as it moves towards the external circuit. The front contact, the emitter, the base and the back contact all have resistance. The total resistance for the conducted electricity are all of the above mentioned resistances in series and called series resistance [33]. Depending on how the solar cell is manufactured, there will be some current that leak over the pn-junction. Shunt resistance is the resistance over the pn-junction. Higher shunt resistance gives lower leakage. A good solar cell has low series resistance and high shunt resistance. Recombination losses happen if the electron hole pair recombine before the electron or hole moves in the external circuit. Recombination can occur in the bulk of the material or at the surfaces. Production error may allow electrons to move between layers. When that occurs, the recombination losses increase.

### Temperature dependence

The efficiency changes with temperature. Lower temperature gives higher efficiency. One equation to calculate the efficiency at different temperatures is given in [24] and [12].

$$\eta_c = \eta_{STC}\left[1 - \mu\left(T_a - Tc, STC + G_T\frac{T_{c,NOCT} - T_{a,NOCT}}{G_{NOCT}}(1 - \eta_{STC})\right)\right] \tag{2.2.3}$$

Here, STC stands for standard test conditions and NOCT stands for nominal operation cell temperature. STC and NOCT is given:
STC:

- cell temperature $Tc, STC = 25°C$
- irradiation $G_{STC} = 1000w/m^2$
- air mass $AM = 1.5$

NOCT:

- ambient temperature $T_{a,NOCT} = 20°C$
- Irradiation $G_{NOCT} = 800W/m^2$
- Wind velocity $\upsilon = 1m/s$
- Back side Open

$G_t$ is the measured irradiation, $T_a$ is the measured ambient temperature. The last two variables are efficiency under STC, $\eta_{STC}$ and the cell temperature under NOCT, $T_{c,NOCT}$ that is collected from solar cell data sheet.

### 2.2.4 Solar movement

From the earth point of view, the sun moves over the sky from east to west during the day. How much sun there is at a location depends on where the location is, which day of the year and what the local time is. The earth is tilted compared to the sun. The tilt is called declination angle. Two days a year the declination angle is zero, the rest of the year it changes between $+23.45°$ and $-23.45°$ according to:

$$\delta = sin^{-1}\left(sin(23.45°)sin(\frac{360}{365}(d-81))\right) \tag{2.2.4}$$

where d is day of year starting with 1. January.

There are 24 time zones across the earth. The earth is divided into 360°, giving each time zone 15°. Local standard time meridian (LSTM) is the meridian for each time zone and is given by

$$LSTM = 15°\Delta T_{GMT} \tag{2.2.5}$$

where $T_{GMT}$ is the difference of the local time compared to Greenwich time.

Equation of time (EoT) is an equation that corrects the eccentricity of the Earth's orbit and Earth axial tilt:

$$EoT = 9.87sin(2B) - 7.53cos(B) - 1.5sin(B) \tag{2.2.6}$$

where

$$B = \frac{360}{365}(d-81) \tag{2.2.7}$$

Both LSTM and EoT are used together with the longitude to calculate the time correction factor (TC). TC corrects for variation inside the time zone.

$$TC = 4(longitude - LSTM) + EoT \tag{2.2.8}$$

From this, the local solar time (LST) is calculated to adjust for the local time (LT).

$$LST = LT + \frac{TC}{60} \tag{2.2.9}$$

Hour angle (HRA) is the sun's position at the sky compared to solar noon. In the morning, the HRA is negative, at solar noon, HRA=0, and at the evening, HRA is positive. HRA is given by:

$$HRA = 15^{\circ}(LST - 12) \tag{2.2.10}$$

When all this is calculated, the sun's elevation(EL) and azimuth(AZ) can be calculated.

$$elevation = sin^{-1}\left(sin(\delta) * sin(latitude) + cos(\delta) * cos(latitude) * cos(HRA)\right) \tag{2.2.11}$$

$$azimuth = cos^{-1}\left(\frac{sin(\delta)cos(latitude) - cos(\delta)sin(latitude)cos(HRA)}{cos(elevation)}\right) \tag{2.2.12}$$

The above equations are from [15].

### 2.2.5 Orientation and tilt

The total amount of radiation is called global radiation, and consists of direct radiation and diffuse/reflected radiation. Diffuse radiation is radiation that hits particles in the sky and spread in all directions. The orientation is defined as azimuth angle(az), where az = 0 is towards north, az = 90 is towards east and so on, following the compass directions. Tilt as

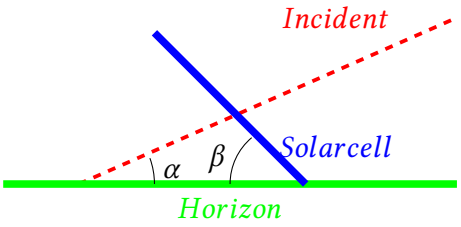


**Figure 2.15:** Solar incident

angle of height from the horizontal plain. To produce maximum power from the solar cell, the direct radiation needs to be normal to the solar cell[25].

A pyranometer measures the global irradiation at a horizontal surface. To calculate the incident irradiation from a horizontal measurement equation (2.2.13) is used.

$$S_{incident} = \frac{S_{horizontal}}{sin(\alpha)} \tag{2.2.13}$$

The sun with azimuth AZ and elevation $\alpha$ and a solar panel with azimuth Y and tilt $\beta$ will have irradiation as a function of the incident irradiation according to equation (2.2.14).

$$S_{module} = S_{incident} * [cos(\alpha) * sin(\beta) * cos(Y - AZ) + sin(\alpha) * cos(\beta)] \tag{2.2.14}$$

Equation (2.2.15) is the combination of equation (2.2.13) and equation (2.2.14) and gives the irradiation on the solar panel from the horizontal measurement[15].

$$S_{module} = S_{horizontal} * \frac{cos(\alpha) * sin(\beta) * cos(Y - AZ) + sin(\alpha) * cos(\beta)}{sin(\alpha)} \tag{2.2.15}$$

### 2.2.6 Two-axis tracking

A two-axis tracking system is a system that follows the movement of the sun and orientate and tilt the solar panels accordantly. If the solar panels are facing the sun at any moment, the azimuth of the solar panels will be equal to the azimuth of the sun, Y = AZ. The relationship between the tilt of the solar panel and the elevation is shown in figure 2.15. If the solar radiation is normal to the solar panels, the angle has to be 90°. Therefore $90° - \alpha = \beta$. If this is inserted in to equation (2.2.15), it gives:

$$\begin{aligned}
S_{module} &= S_{horizontal} * \frac{cos(\alpha) * sin(90° - \alpha) * cos(AZ - AZ) + sin(\alpha) * cos(90° - \alpha)}{sin(\alpha)} \\
S_{module} &= S_{horizontal} * \frac{cos(\alpha) * cos(-\alpha) * cos(0) + sin(\alpha) * -sin(-\alpha)}{sin(\alpha)} \\
S_{module} &= S_{horizontal} * \frac{cos^2(\alpha) + sin^2(\alpha)}{sin(\alpha)} \\
S_{module} &= S_{horizontal} * \frac{1}{sin(\alpha)}
\end{aligned} \tag{2.2.16}$$

This is the same as equation (2.2.13) and is the incident irradiation calculated from a horizontal surface.

# 3

# Method

## 3.1 Site

Asko Nord AS is located in Ramfjordbotn south-east of Tromsø in northern Norway, with latitude 69.56°$N$ and longitude 19.14°$E$. This is the location for which the renewable resources are analysed. This is the location of one of two weather stations. The other weather station is located at Holt, south-west on the island of Tromsø, with latitude 69.65°$N$ and longitude 18.91°$E$. At Holt, the Norwegian Institute of bioeconomy research formerly Norwegian Institute for Agricultural and Environmental Research, and Bioforsk collaborate with the Norwegian Meteorological Institute to run and maintains the weather station.

## 3.2 Sensors at Asko

Asko have a Davis Vantage(DV) Pro 2 weather station installed. The standard DV Pro 2 has a rain collector, thermometer, humidity sensor and anemometer. In addition, Asko have a solar radiation sensor. The weather station is mounted on a pole on the north corner of a maintenance house on the flat roof of Asko's warehouse. This is not a good placement for wind measurements. Figure 3.2 shows the roof at Asko, and the red ring is the location of the sensors. The weather station was installed late in the summer of 2013. The station is operated by the IT-coordinator at Asko. The IT-coordinator checks the software on


**Figure 3.1:** Map of Asko Nord and Holt. Map from `kartverket.no`

a weekly basis and has a visual check if the software shows indications of malfunction.

### Davis Vantage Pro 2 anemometer

The DV Pro 2 anemometer measures wind speed and wind direction. The wind speed sensor consists of wind cups and a magnetic switch. The wind speed is calculated from 1600 revolutions per hour, which equals 1 mile per hour (mph).

$$V = P(\frac{2.25}{T}) \tag{3.2.1}$$


**Figure 3.2:** Aerial photo over Asko's area. photo from kartverket.no

Where V is the wind speed in mph, P is number of pulses per sample period and T is sample period in seconds. The measurement is converted to the nearest 0.1 $m/s$. The range is 0.5 to 89 m/s and the accuracy is ±2 $mph$, ±1 $m/s$ or ±5 % whichever is greatest[8]. The direction is determined by a wind vane and a potentiometer. The potentiometer has a resistance between 0 and 20Ω where 10Ω equals south[8]. The direction has a resolution of 1° and range from 0° to 360° and a nominal accuracy of ±3° [9].

## 3.3 Sensors at Holt

Of relevant measurements, Holt measure temperature, solar intensity, wind velocity and wind direction. The weather station was established in 1987 and has collected data from 1. June 1987. The Holt station delivers data to Norwegian Meteorological Institute and is a part of their system for quality control. They control check if the data is inside a given interval, that the steps are not too large compared to the previous value, and that the measured parameters are logical together. The station is controlled and calibrated once a year[30].

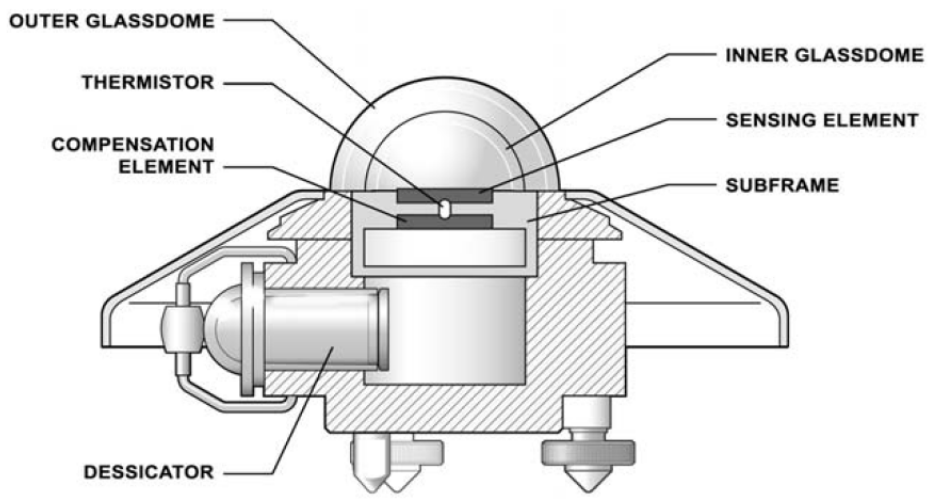


**Figure 3.3:** Illustration of the CM 11 pyranometer from Kipp and Zonen. Figure from [21]

### 3.3.1 CM 11 pyranometer

Holt have the CM 11 pyranometer from Kipp and Zonen [14]. Light passes through the two glassdomes and the energy gets absorbed by a black painted disk. Between the disk in the glassdomes and a heat sink, there is thermal resistance. The difference in temperature produces a voltage over the thermal resistance that is used to calculated the energy[21]. Output unit calculated is in $W/m^2$. Figure 3.3 illustrate the components of CM 11. The International Standard Organisation (ISO) have listed CM 11 as secondary standard according to ISO 9060 [21].

## 3.4 Data collection and manipulation

### 3.4.1 Asko

All of the wind data is collected from the David Vantage pro 2 weather station. The station is not professional and downtime will happen. The main data set used in this thesis is collected from 20.10.2014 to 20.10.2015, supplied with all other available data. For wind, each set is processed in the following way:

- If there are hours with two or more samples, the average for the whole hour is calculated for both wind speed and wind direction.

- If the wind direction is above 360 degrees, the values are faulted.
- If both the wind speed and wind direction are zero, the valued are faulted.

Without the last point, almost 20 % of all data would have been with zero wind speed and pointing straight north. Based on other observations and the instability of the weather station, this is faulted as an abnormality.

### 3.4.2 Holt

All the data from Holt is collected at Agrometeorology Norway, `lmt.nibio.no`. The data is hourly average, starting 1. January 2006 and ending 31. December 2015. The hours with missing data are replaced with the mean of the same hours from the remaining years. The data is summarized in weeks and months, with 1. January being day one in week one. In leap years 29. February is considered as 1. March and the last day of the year is unused. The wind speed distribution is calculated for each year from 2006 to 2015, and the Weibull distributions are calculated with the equations in section 2.1.2. For sun, the mean and standard deviation are calculated

## 3.5 Wind calculations

### 3.5.1 Horizontal wind shear

From section 2.1.4, the the wind share exponent change under different conditions in known. Upon lack of measurements to determine the wind share exponent, table 2.1 has been used. Asko is not in one of the specific conditions in the table. Close to the warehouse there most likely is some turbulence. At a distance above the warehouse, the wind is probably closer to neutral or stable. In the surroundings is another warehouse and some trees, and the sea is close by. It is not trivial to determine the initial height. The warehouse is 15 meters high, and as told in section 3.3, the measurement is not placed on the edge of the roof. Based on the fact that the measurement is placed at a distance from the edge of the warehouse, the initial heigh is set to two meters. Wind at ten meters height is calculated with share exponent $\alpha_1 = 0.06$, $\alpha_2 = 0.14$ and $\alpha_3 = 0.27$.

### 3.5.2 Flow design

Flow design is a wind simulation program from Autodesk. The program uses CFD to create a virtual wind tunnel. In the wind tunnel, airflow is visualized

around CAD structures. To solve the air flow design use finite volume method and for turbulence LES is used. Flow design is geometrical tolerant and not sensitive to imperfections in the CAD model[3].

### Flow design parameters

Flow design is not the most sophisticated wind simulation program. The configurations the user is able to change are limited to:

- Import an CAD model
- The wind tunnel bounds are changeable with drag / pull buttons.
- The simulation resolution from low (50%) to high (400%).
- 2D or 3D simulation.
- Orientation of simulated model.
- The wind speed into the tunnel.

There are some more options that handle how the result is shown, such as plane, surface pressure, vectors, etc. Boundary conditions, wind profile or wind speed at an array is not a option.

The reason for doing the Flow design wind simulation is to find out:

- If the wind speed measured is too low or too high or gives a correct picture of the wind in the area.
- The behaviour of turbulence in the area.
- If there are places that are more fitted for wind turbine than others.

### Input Flow design

The input selected is:

- Wind tunnel with length approximately one and a half length of the model in front, two lengths of the model in the back and half the width on each side.
- Simulation resolution to 100%.
- 3D simulation.
- Orientation and wind speed changes to cover the distribution of wind.

At every simulation some results are saved: three planes in the wind direction. One over the measurement, one on the middle and one over the ventilation on the north side of the building. Some planes normal to the wind direction. One or two vertical planes a distance over the building. And some isosurfaces.

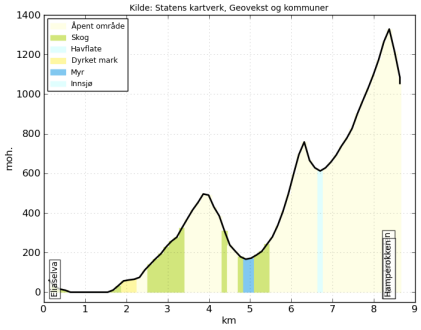


**(a)** Height profile for line two

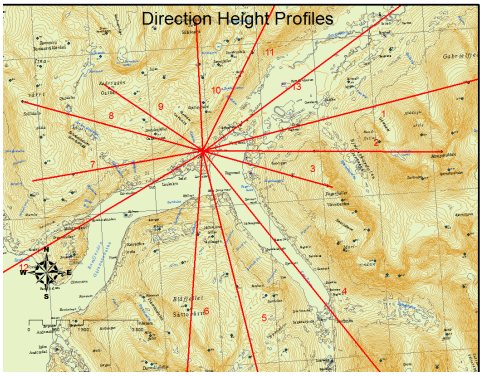


**(b)** Directions of height profiles

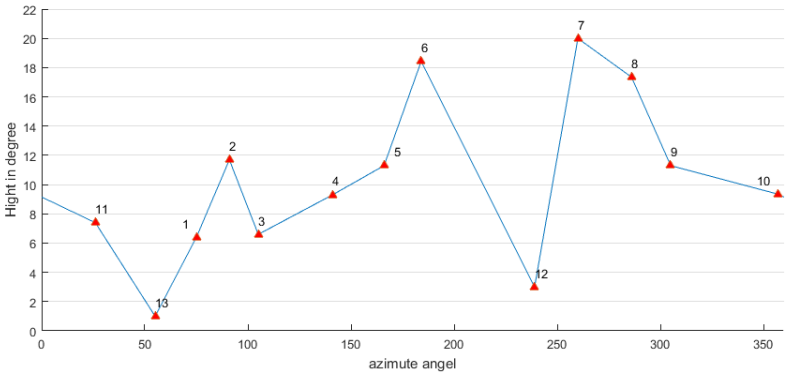


**(c)** Height for the corresponding lines

**Figure 3.4:** Shadowing

## 3.6 Solar calculations

### 3.6.1 Shadowing

Asko is located in the end of a valley with mountains in several directions. When the sun is either under the horizon or behind a mountain, the direct radiation is zero and the measured global radiation is diffused. Figure 3.4a shows a height profile from kartverket.no for line two in figure 3.4b. From this, the height in degree $el$ from Asko to the surrounding mountains are possible to calculate using the following equation:

$$el = arctan(\frac{height}{length}) \tag{3.6.1}$$

This is done for all of the lines in figure 3.4b, and the result is shown in figure 3.4c. The red dots are calculated values and the blue line is the estimated line of shadow from the surrounding mountains.

### 3.6.2 Energy from solar panel

From the data collected from Holt, the mean solar irradiation and mean temperature for each hour are calculated. With the equation in 2.2.4, the solar elevation and azimuth for the same hours are calculated. The measured radiation is the global radiation at a horizontal surface. The portion of direct and reflected or diffused radiation depends on multiple factors. The two most significant factors are clouds and shadowed sun. The first factor is not handled here. The second factor is discussed in 3.6.1. The plot in figure 3.4c is converted into an equation. The equation inputs azimuth and gives the height of the blue line. According to Solanki [38] the diffused part of a global radiation is 15 % to 20 % on a clear day. On a cloudy day, the diffused fraction is, depending on the clouds, larger. To compensate for the cloudy days and reflected irradiation, the direct irradiation is assumed to be 75 % of the measured when the sun is not shaded by the surrounding mountains. When the sun is shaded, all the measured radiation is set to be reflected or diffused.

#### Orientated and tilted panels

If solar panels are orientated and tilted, the direct part of the irradiation can produce more energy according to (2.2.15). The total irradiation on the solar panel is the diffused or reflected and the calculated irradiation on the plane from the direct radiation. To find the optimal orientation and tilt, for each combination of orientation between 0° and 360° and tilt between 0° and 90° the energy is calculated.

#### Two-axis system

To calculate the irradiation on the two axis system, the irradiation on the two-axis solar panels, in similar to orientated and tilted, the diffused or reflected and the calculated irradiation on the plane from the direct radiation from equation (2.2.16).

#### Efficiency

To calculate the energy produced, each square meter of tilted solar panels and the two-axis panels the total irradiation is multiplied with the efficiency found in equation (2.2.3). $\eta_{STC}$ and $T_{c,NOCT}$ are unknown in equation (2.2.3), therefore as an example, data for Benq solar SunForte 327W [39] is used, $\eta_{STC} = 0.201$ and $T_{c,NOCT} = 45°C$.

# 4

# Results and discussion

## 4.1 Raw wind data

The raw wind data is collected from both Asko and Holt.

### 4.1.1 Asko

Figure 4.1 shows the collected data from Asko's measurements. The blue lines are the measured average data and the red bars are the hours without data. There are a total of 8760 hours in a normal year. In the set, there are 7397 hours and 1363 hours with missing data, giving a total of 15 % missing data. There are two periods with large holes. The first is from around hours 2000 to 3000, late Mars to early May. In this period, there are small periods with recorded data. In the second period from about hour 4300 to 4800, the majority of June, most of the data is missing. The rest of the hours without data are spread out through the set in small bulks.

Figure 4.2 shows: the distribution of collected hours, the Weibull distribution, and mean for both the measured values and the Weibull distribution.

From the collected data, the distribution of wind speed and direction is shown as a wind rose in figure 4.3. The wind rose shows that the majority of the wind comes from the west and the east. Figure 4.4 shows the wind rose placed on top of the over the area. The illustration shows that the strongest winds come

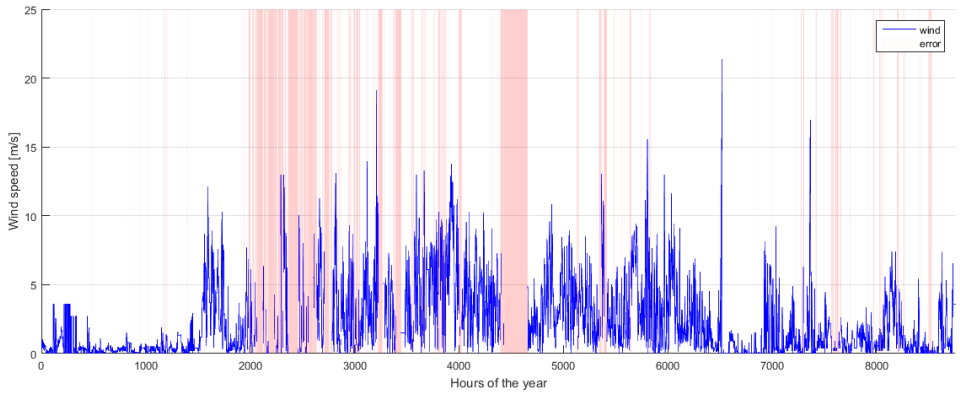


**Figure 4.1:** The blue line is the average wind speed at different hours during a year. The red bars are hours with missing data

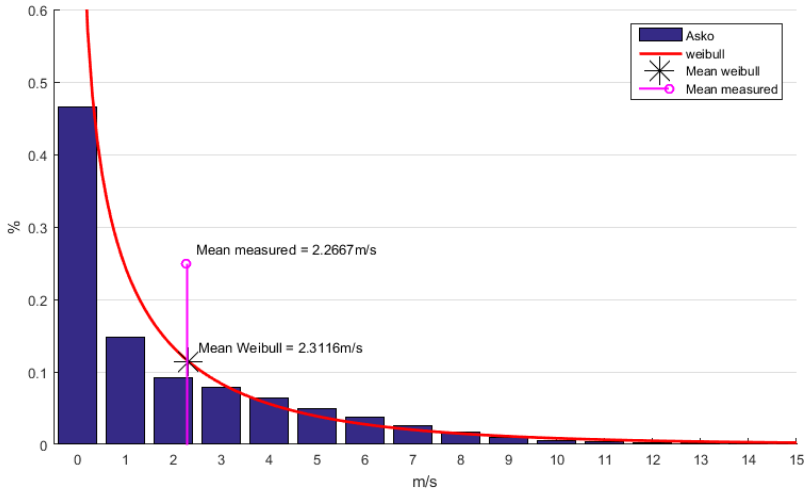


**Figure 4.2:** Wind distribution and Weibull distribution at Asko

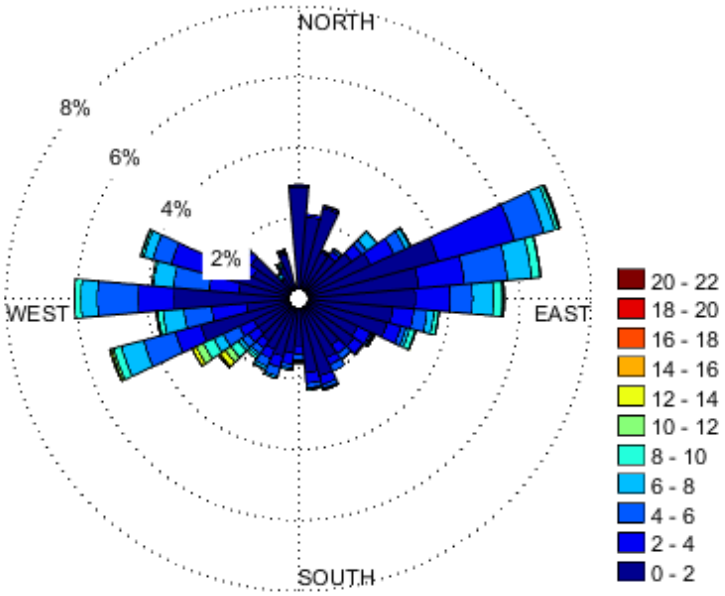


**Figure 4.3:** Wind rose showing the distribution of wind speed and wind direction from the weather station at Asko

from the open area towards the sea and from the valley.

### 4.1.2 Holt

The wind distribution and Weibull distribution for the measurement period is shown in figure 4.5. For 2015, the wind rose plot in figure 4.6 shows the distribution of wind speed and direction. This is placed together with the wind rose from Asko in figure 4.4. This shows that at Holt, the majority of the wind comes directly from the south where there are open seas and no mountains. The wind distribution for Asko is different from the one for Holt, and yet the distribution and mean might be useful to compare. The Weibull distribution at Holt is shaped more like a Rayleigh distribution than the one for Asko, which has an exponential shape. According Seguro and Lambert [36] the Rayleigh shape is more common than the exponential shape. This might indicate that the measured wind speed at Asko can be abnormally low. This is noted. For the

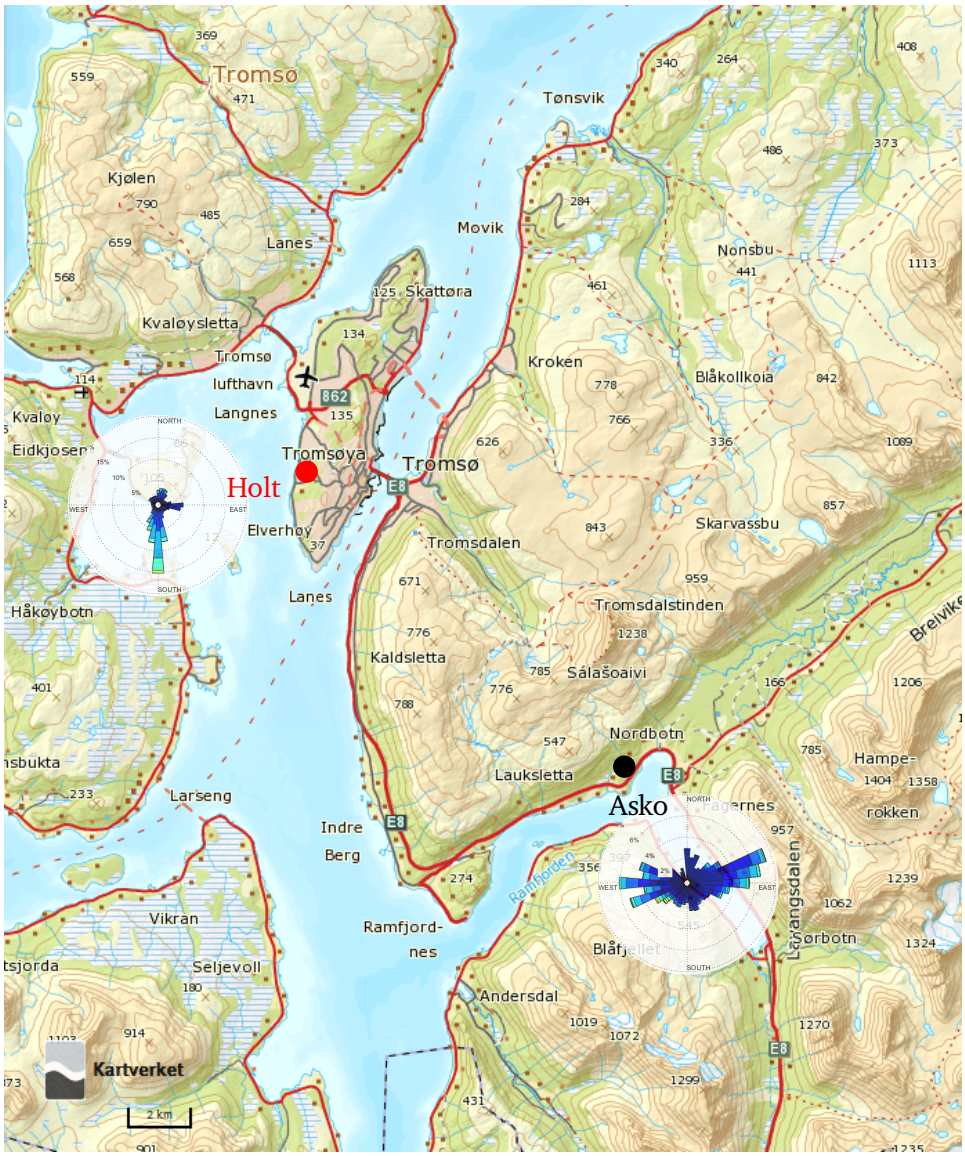


**Figure 4.4:** Wind direction compared to the surroundings [photo from kartverket.no]

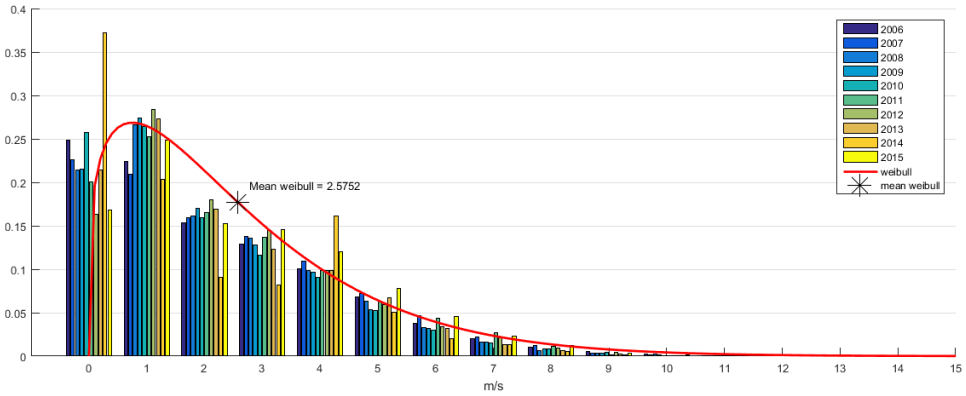


**Figure 4.5:** The wind distribution for the year 2006 to 2015 and weibull distribution for all the years

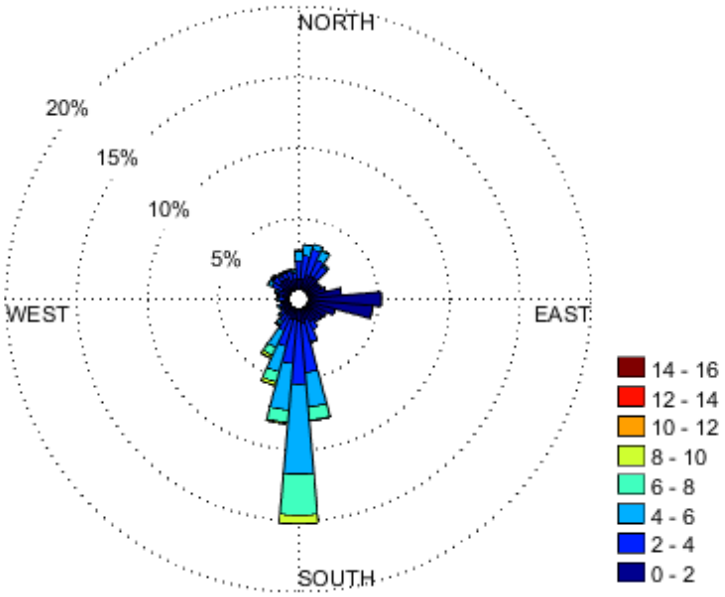


**Figure 4.6:** Wind rose showing the distribution of wind speed and wind direction from Holt

remainder of this thesis, only the measurements from Asko is used.

## 4.2 Wind share exponent

The wind distributions and rose distributions for the different share exponents are shown in figure 4.7. As the share exponent increases, the distributions show more hours with higher wind speeds and an increase in mean wind speed. As previously discussed in section 2.1.4 and section 3.5.1, the wind share exponent is hard to determine. The site is a semi urban area with some surrounding objects. Due to lack of lack of a calculated value, $\alpha = 0.14$ is selected as a mean.

## 4.3 Flow design results

From the distribution of wind with different share exponents shown in figure 4.7 the input direction and wind speed chosen for the simulation is as follows:

| Orientation | wind speed |
|---|---|
| 0° | 1 m/s |
| 70° | 6 m/s |
| 80° | 3 m/s, 6 m/s, 10 m/s |
| 90° | 6 m/s, 10 m/s, 15 m/s |
| 180° | 1 m/s |
| 240° | 15 m/s |
| 250° | 6 m/s, 10 m/s |
| 270° | 3 m/s, 6 m/s, 10 m/s |

All the input wind speeds are constant at all heights due to program limitations. The majority of wind with high wind speeds are from two bulks. The first bulk is from the east, between 65° and 95°. The second bulk is from the west, between 235° and 275°.

The scale inside Flow design display sixteen intervals. The scale's minimum value is zero and the maximum value is the maximum wind speed $v_{max}$ in the simulation. The boundary b between the intervals is determined by the formula

$$b_n = v_{max}\sqrt{\frac{n}{16}} \tag{4.3.1}$$

where n is the boundary number, starting with zero and ending with sixteen.

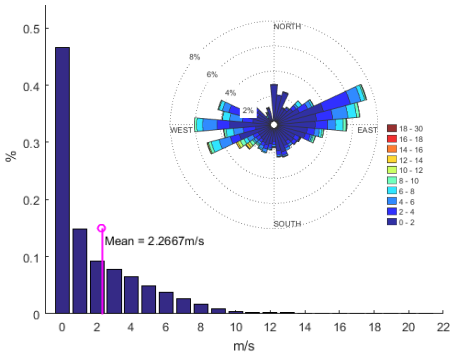


**(a)** Wind share exponent = 0

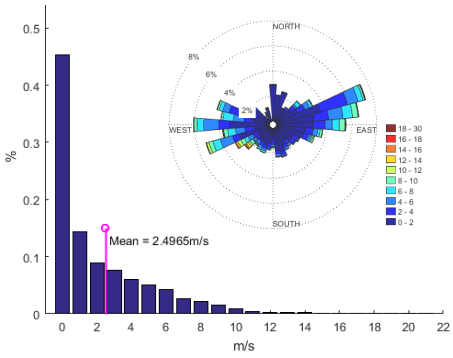


**(b)** Wind share exponent = 0.06

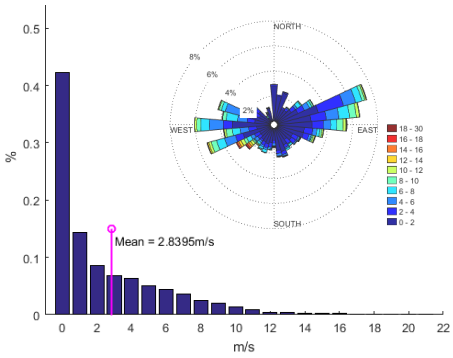


**(c)** Wind share exponent = 0.14

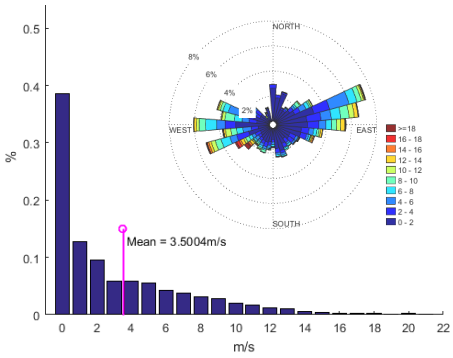


**(d)** Wind share exponent = 0.27

**Figure 4.7:** The wind distribution displayed as a percentage of the speed and wind rose for changing wind share exponent

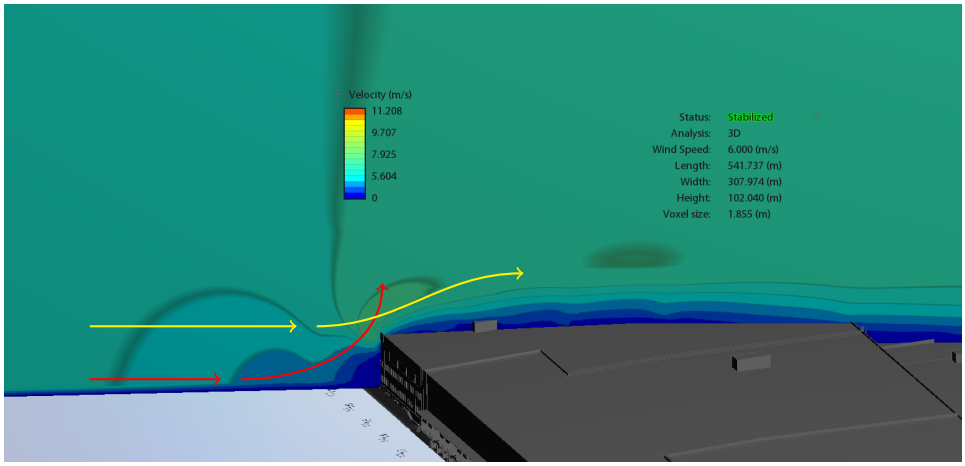


**Figure 4.8:** The red lines show wind flowing upwards, that meets the yellow line and creates the blue field with low wind speed close to the roof. The orientation in this simulation is 70° and the wind speed is 6 $m/s$.

### 4.3.1 East bulk

The north-east side of the building is, as shown in page 25, figure 3.2, straight with an additional square office building at the eastern end.

#### Wind measurement

The wind sensor is close to the north-east wall. The first red arrow in figure 4.8 is wind moving towards the north-east wall at low height and will not be able to pass into the wall and will have to stray away from the wall. Some of the air moves to the sides if there is room, other moves upwards, shown as the last part of the red arrow in the figure. The wind moving towards the roof at roof height meet the upwind and change direction somewhat upwards. This creates a belt with less wind close to the roof as shown in the blue part of the figure. The example in figure 4.8 is for wind from 70°, and simulations with wind from 80° and 90° shows similar results. Figure 4.9 is a close-up of the location of the wind sensor. The wind sensor is not included in the simulation, but the location is illustrated with a red arrow. The yellow arrow shows the scale color seen at the red line. The wind speed in that section is between 12.14 $m/s$ and 13.31 %. The input wind to the simulation is 15 $m/s$ and constant at all heights. Hence, it is possible to conclude that with wind from this bulk, the wind measurement will read lower values than the actual wind coming from the east.

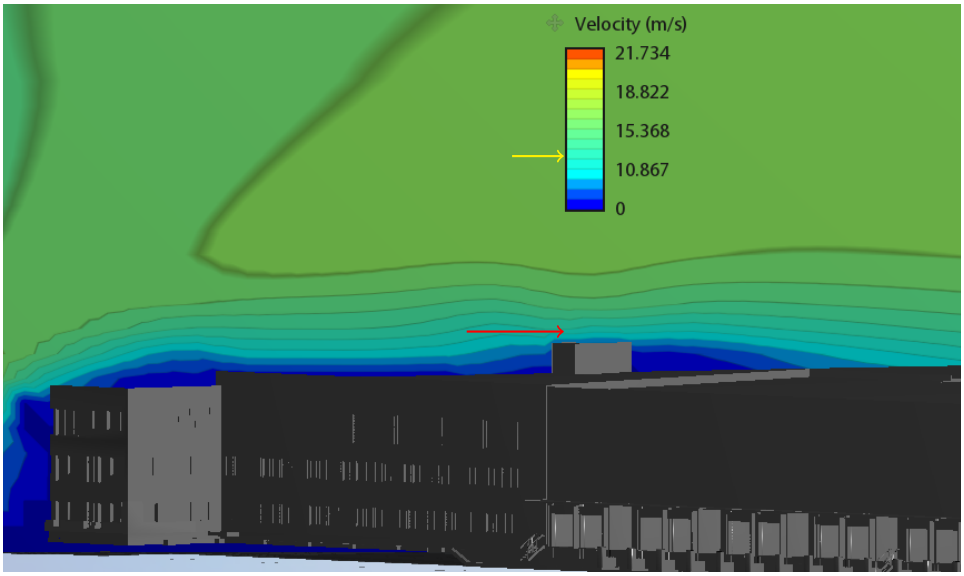


**Figure 4.9:** Closeup of the location of the wind sensor. Simulation with orientation 90° and wind speed 15 $m/s$. The red arrow indicates the location of the wind sensor.

### Turbulence

The easterly winds have meet a fairly straight wall. From this side, the simulation shows two main reasons for turbulence. The first is the section with low wind speed near the roof, as discussed in the above section and shown in figure 4.8. The second factor is the protruding structures on the roof, i.e. maintenance houses, garage and fans. The turbulence behind the fans is shown in figure 4.10, where the plane follows the wind direction. The wind in that figure comes from 90° and the wind speed is 10 $m/s$. The amount of turbulence depends on the wind speed. Figure 4.11 is from 80° and with wind speed 3 $m/s$. The plane is cut normal to the wind direction. Behind the obstacles on the roof, it is possible to see the signs of turbulent flows.

### Placement of wind turbine

Wind turbines do not work optimally in turbulence, and the wind is normally not at its strongest in turbulent areas. The areas with enhancement of wind is more attractive. Figure 4.8 figure 4.9 and figure 4.10 have a area stretching from the north-east wall over the roof and turbulent air, that have higher wind speed than the input to the simulation. In figure 4.12 a) and b), the limit of the isosurface is 16.6 % higher than the input, and as the figures show, there is large area with this enhancement as a minimum. Figure 4.12 show the same

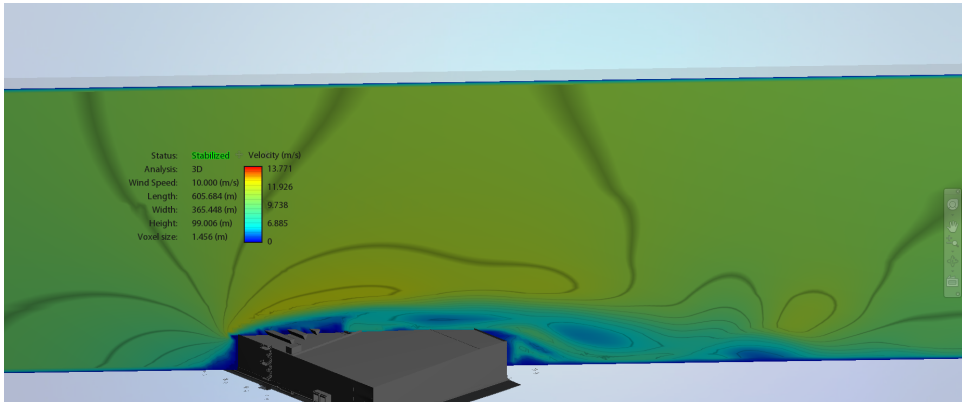


**Figure 4.10:** Plane that cuts normal to the wind direction. Wind comes from 90° and wind speed is 10 $m/s$

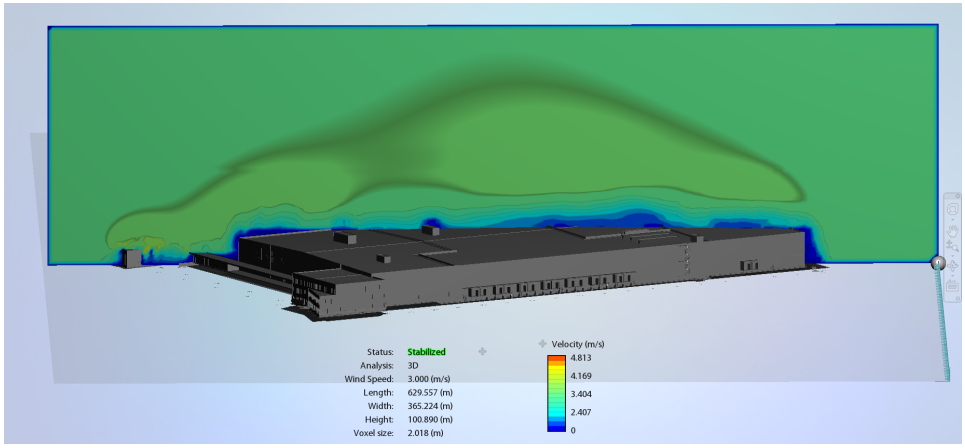


**Figure 4.11:** Plane that cuts normal to the wind direction. Wind comes from 80° and wind speed is 3 $m/s$

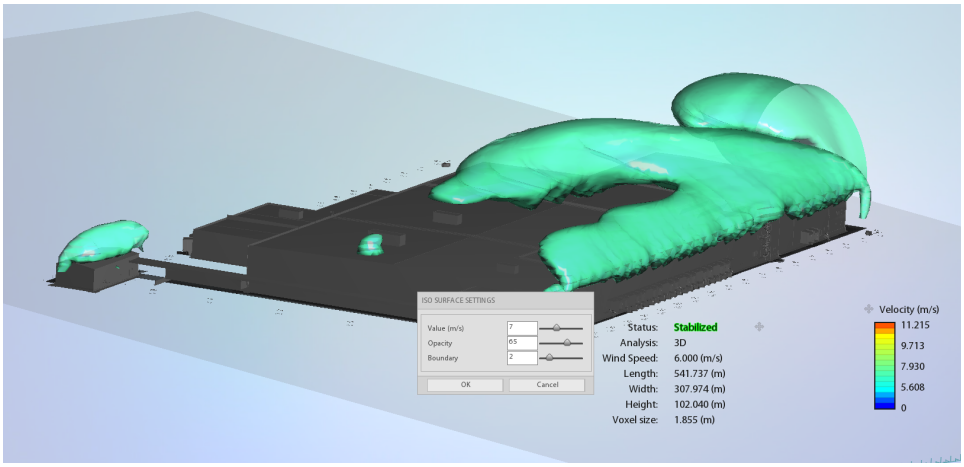


**(a)** wind from 70°, wind speed 6 $m/s$ and isosurface limit at 7 $m/s$

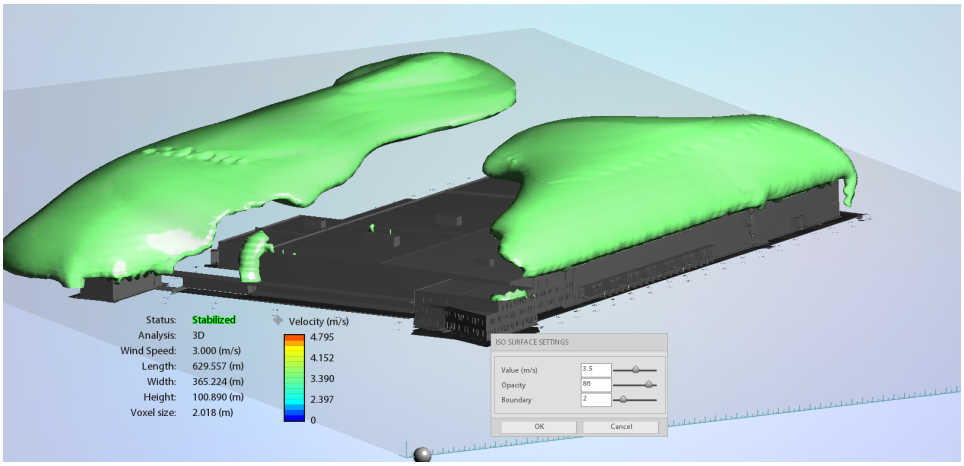


**(b)** wind from 80°, wind speed 3 $m/s$ and isosurface limit at 3.5 $m/s$

**Figure 4.12:** Isosurfaces from easterly winds

isosurface from two different directions: a) from the side and b) from above. The limit for the isosurface is in this case 20 % higher than the input. From the red scale it is possible to see that the isosurface starts at a height of 1.5 of the height of the building and the ends at about 2.15 of the height. The majority of enhanced wind is in this case between the 1.5 $h$ mark and the 2.0 $h$ mark.

### 4.3.2 West bulk

The south-west side of the building does not have a straight wall. There are smaller sections covering the side making corners both inwards and outwards,

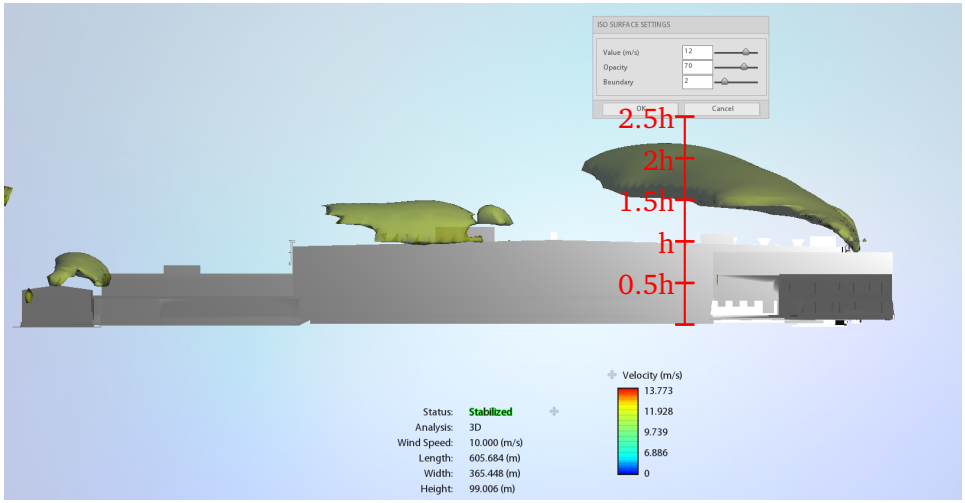


**(a)** Side view of isosurface.

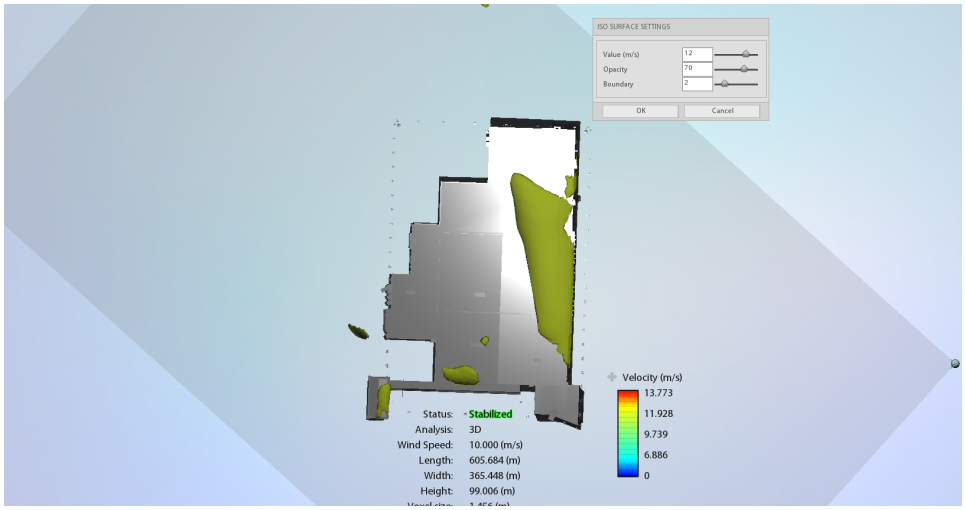


**(b)** Top view of isosurface.

**Figure 4.13:** Side view and top view of the same isosurface with wind from 90°, wind speed 10 $m/s$ and limit 12 $m/s$

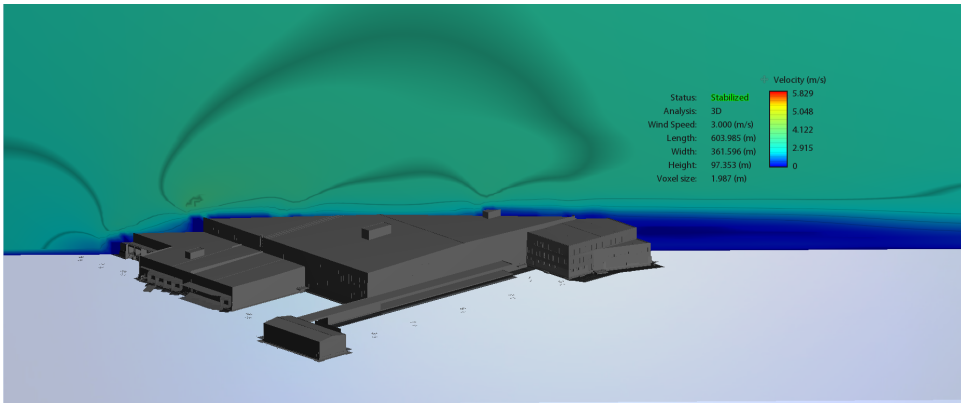


**(a)** Wind from 270° and wind speed 3 $m/s$. The plane follows the wind direction

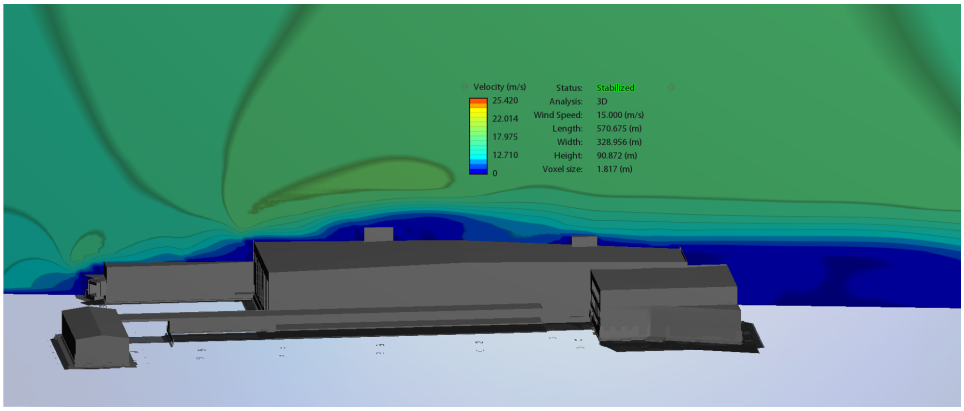


**(b)** Wind from 240° and wind speed 15 $m/s$. The plane follows the wind direction.

**Figure 4.14:** The effect on wind from west on the measurement site

as shown in page 25, figure 3.2.

### Wind measurements

Wind from the west side need to pass the edges and corners on the way to the wind sensor that is closer to the north-east side of the building. From figure 4.14a it could be interpreted that wind at the sensor is not affected by the building as the wind from east. However, this is not correct for all westerly winds. From for example wind from 240° shown in figure 4.14b. Here one of the maintenance houses is directly in front of the sensor. The house makes a turbulent area behind it, making a large effect as observed in the figure. In this case the wind sensor is likely to measure too low wind speeds.

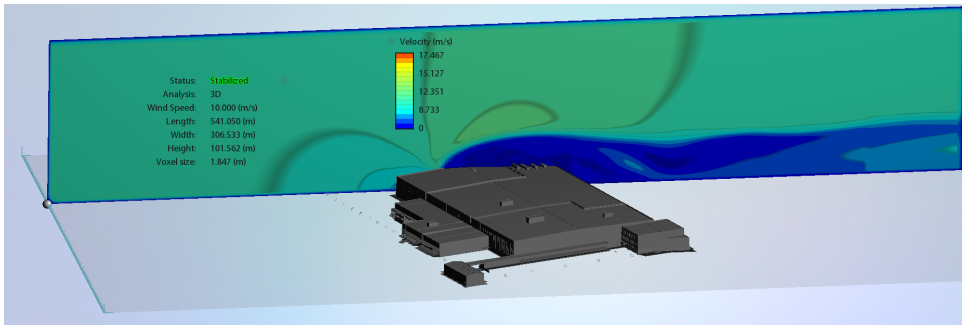


**(a)** Wind from 250° and wind speed 10 $m/s$. The plane follows the wind direction.

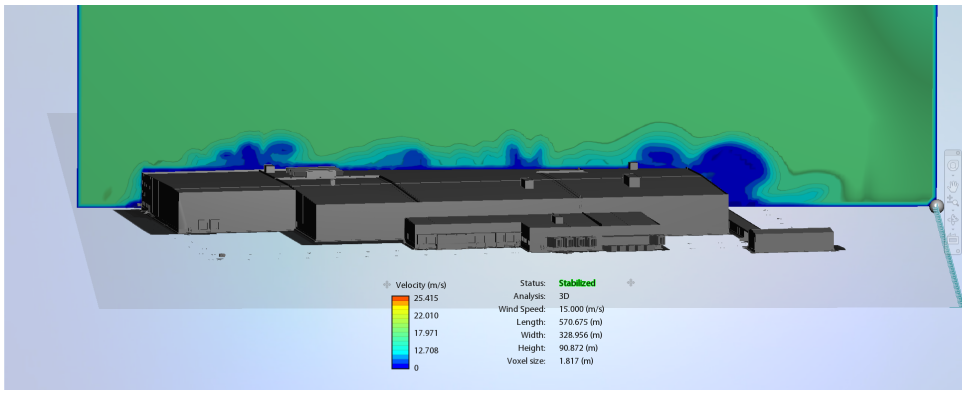


**(b)** Wind from 240° and wind speed 15 $m/s$. Plane normal to the wind direction.

**Figure 4.15:** Figure to illustrate turbulence from the west bulk

### Turbulence

Due to the south-west wall, the wind moving from west is forced into inwards corners. In the corners, wind is forced upwards. In the same way as the wind in figure 4.8, the wind moving upwards meet wind moving in the wind direction. This creates an area behind the corners where wind might be turbulent. This is shown in figure 4.15a, where there is a large blue field behind the corner. The wind direction is changed from 250° to 240° in figure 4.15b. Here, the plane is normal on the wind direction. The turbulence from all the inward corners is shown as blue areas in the plane behind. Additionally, the effect from the protruding structures is also shown in the plane.

### Placement of wind turbine

As in section 4.3.1 the location of the wind turbine is optimal where the wind is enhanced. The effect of enhanced wind speed starting at the wall facing the wind and above the turbulent air is similar from both directions, as can be seen

in figure 4.14a, figure 4.14b and figure 4.15a. However, the the turbulence is different and has a larger effect from this side. This is exemplified in figure 4.16b where the area high over the turbulent north corner is inside the limit of the isosurface. The wind speed into the simulation is in this case 10 $m/s$ and the limit of the isosurface is 11.5 $m/s$. This gives an minimum of 15 % higher wind speed. Figure 4.16a shows an example where the increase is 16.6 % at a minimum over a larger area. The height of the turbulence stretches to about 2.5 times the height of the building for the north corner according to figure 4.17. As shown by the yellow line, the turbulent area from the other sources does not pass the $2h$ line.

### 4.3.3 Summary of simulation

The simulation confirmed that the location of the wind sensor is not ideal. The measured wind speed is significant lower than the wind into the simulation. The easterly wind measurement is affected by a belt of low wind, and the westerly wind measurement is affected by turbulence from the inwards corners or protruding structure.

The isosurface simulation from the east side shows that the wind is enhanced the most over the wall facing the wind. The side planes however show that there is an area with enhanced wind stretching further back and somewhat up. The enhancement is not as strong as directly above the wall, but still significant. From the west, it is shown that the wind is most enhanced above the area with turbulence. This is somewhat hard to handle when the direction of the wind changes the location of turbulence. It is observed that over two times the height of the building most turbulence is avoided. The north corner is the exception.

When combining the results from the simulation, it is shown that a wind turbine placed at two times the height of the building, approximately 15 meters over the roof, can be placed in the blue area in figure 4.18. The red area shows where additional height is recommended.

Exactly how much more wind the wind turbines will experience is hard to determine. Some calculations have shown that the measurement is 15 % lower than the input to the simulation, and others have shown that the enhanced area more than 15 % above the input to the simulation. This suggests that overall the wind measured is too low compared to the potential for a wind turbine.

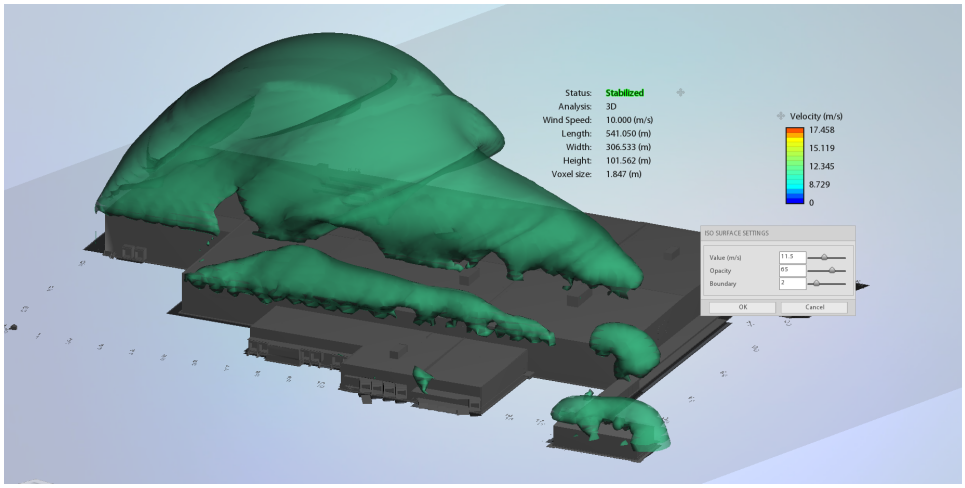


**(a)** Isosurface with limit 11.5 $m/s$. The wind into the simulation is 10 $m/s$ and the direction is 250°

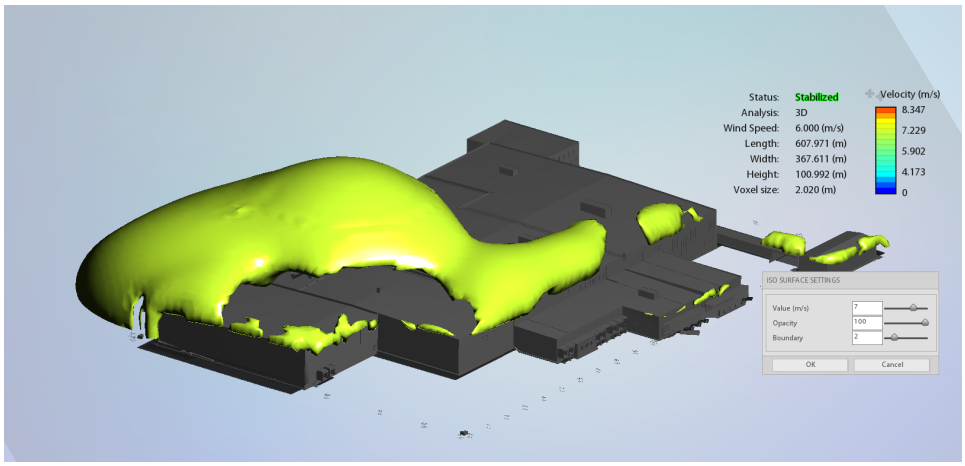


**(b)** Isosurface with limit 7 $m/s$. The wind into the simulation is 6 $m/s$ and the direction is 270°

**Figure 4.16:** Isosurface from westerly winds.

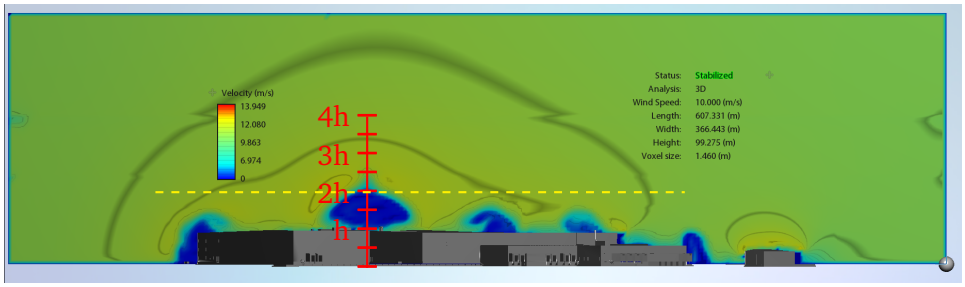


**Figure 4.17:** Wind from 270°
and wind speed 10 $m/s$. The plane is normal to the wind direction.

**Figure 4.18:** Aerial photo over Asko's. The blue section indicates the area where the majority of the turbulence is below twice the height of the building, and the red section indicates the area where the turbulence have a tendency to be above twice the height [photo from kartverket.no]

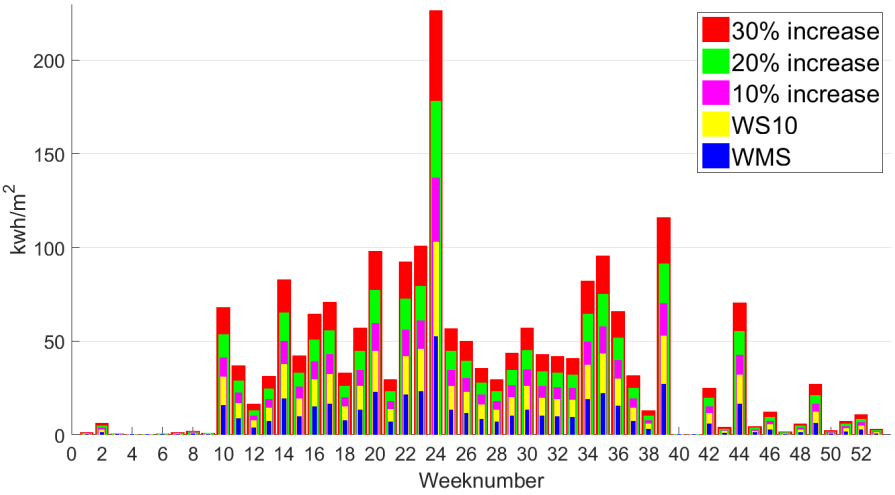


**Figure 4.19:** The energy from wind for each square meter. The dark blue bars are measured values. The rest are with different increase percentages.

## 4.4 Power from wind

The energy in wind is given from equation (2.1.8). The measured wind speed (WMS) is increased to estimate the wind at ten meters height (WS10) according to section 4.2 with wind share exponent $\alpha = 0.14$ . From section 4.3.3 it is shown that the wind will be enhanced if the turbine is located at optimal locations. Therefore, the WS10 is increased with 10 %, 20 % and 30 %. For WMS, WS10 and each of the increased wind speeds the energy is calculated. The hours without wind speed is given the mean energy of all the collected wind speeds. Figure 4.19 shows the energy in kWh from wind for each week.

The change in wind and energy is summed up in table 4.1. This shows that the energy in the wind is 334 % higher at the best case compared to the energy from MWS.

| Increased wind | Average wind | Total energy(year) | Increased energy |
|---|---|---|---|
| MWS | 2.26 $m/s$ | 471 $kWh/m^2$ | 0 % |
| WS10 | 2.83 $m/s$ | 930 $kWh/m^2$ | 97 % |
| 10 % | 3.12 $m/s$ | 1237 $kWh/m^2$ | 163 % |
| 20 % | 3.40 $m/s$ | 1606 $kWh/m^2$ | 241 % |
| 30 % | 3.69 $m/s$ | 2042 $kWh/m^2$ | 334 % |

**Table 4.1:** Summary of change in wind and energy with enhanced wind speed

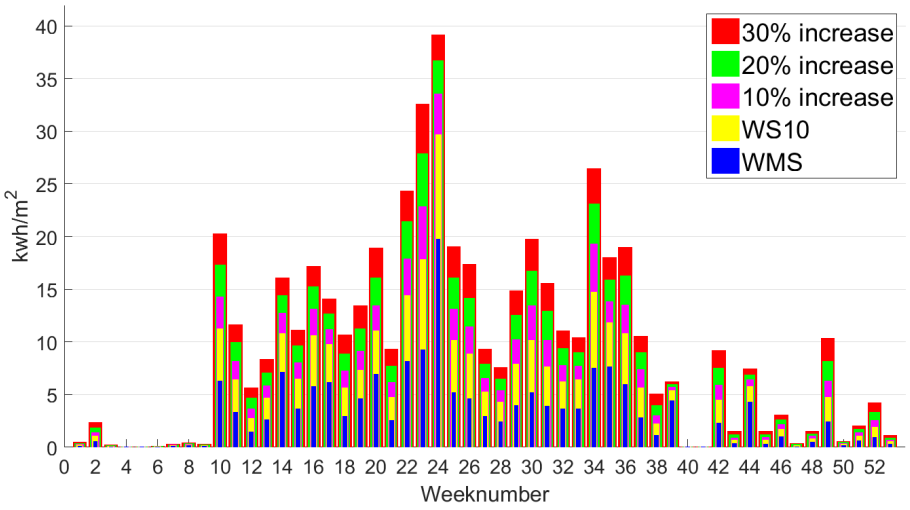


**Figure 4.20:** The theoretical energy of a wind turbine with $C_p = 0.4$ and values for power curve: cut-in = 2.5 $m/s$, rated= 15 $m/s$ and cut-out= 25 $m/s$

### 4.4.1 Energy from wind turbine

The energy in wind is given by equation (2.1.8) and from section 2.1.5 the coefficient of power and the principle with power curve is introduced. In this section, all of this is combined. The same five sets of wind speed as the above section is used. The production is set to zero when the wind speed is under cut-in speed or over cut-out speed. Between the rated speed and the cut-out speed, the production is set to the production at rated wind speed. For any other wind speeds, the production follows the wind speed. The values of the power curve are collected from the example in section 2.1.5. The coefficient of power is set to 40 %. The sum of energy each week is calculate and shown in figure 4.20. The difference between the weeks is large. There are multiple reasons for that. Firstly, in the weeks with low wind speeds, the turbine will operate fewer hours since the wind speeds often will be under the cut-in speed. Secondly, the production depends on wind speed. As noted on section 2.1.3 the energy increases with third power of the wind speed. The yearly production for each sets is: $E_{MWS} = 169\ kWh/m^2$, $E_{WS10} = 296\ kWh/m^2$, $E_{10\%} = 367\ kWh/m^2$, $E_{20\%} = 439\ kWh/m^2$ and $E_{30\%} = 510\ kWh/m^2$.

## 4.5 Raw Solar

The mean measured solar irradiation on a horizontal surface from the collected data for each hour at Holt is shown in figure 4.21. The data collected is converted

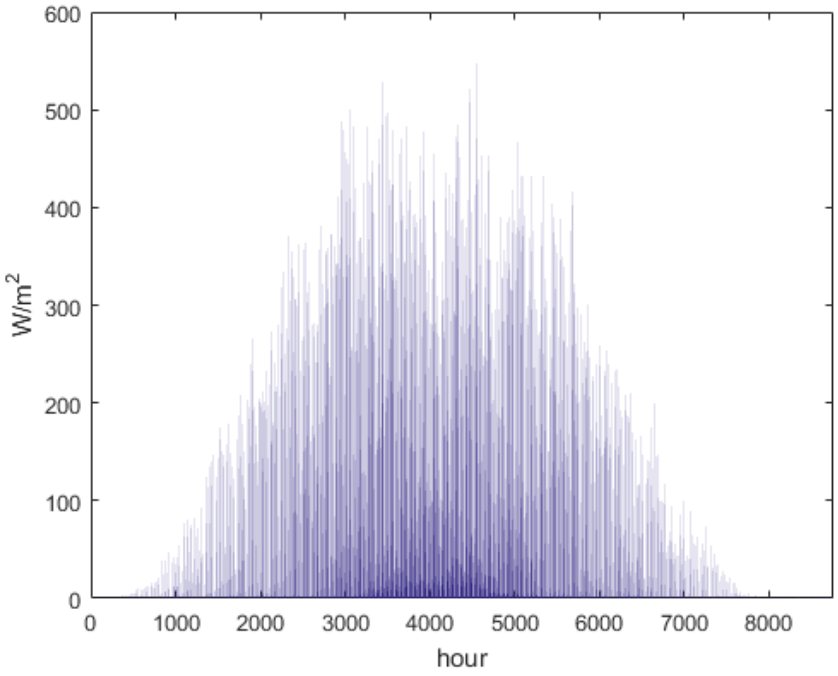


**Figure 4.21:** The measured solar irradiation on a horizontal surface at Holt

to energy, the mean and standard deviation for each week and each month is shown in figure 4.22a and figure 4.22b. The mean total energy for the 10 years is 687.35 $kWh/m^2 \cdot year$ with standard deviation 34.26 $kWh/m^2 \cdot year$.

### 4.5.1 Difference in solar measurement between Asko and Holt

Asko's weather station has measurement for solar irradiation. The station was installed in late in 2013. The collected data have big holes and the data freezes at some points. There are not enough data to have a sufficient set even if all available data is used. Figure 4.23 shows that during hours without error the measurements are quite similar. In the blue Asko data, freezes are not uncommon. This makes the error large in a considerable amount of hours. One example is around hour 500, where the measurement goes from an error value zero to a freeze at almost 300 $w/m^2$ that goes on for many hours during the night when there was no sunlight. The black line shows that the difference is largest at periods when the Asko data is frozen. Since the measurement from Asko is poor and the difference between Asko and Holt is small, the dataset from Holt is used in future calculations.

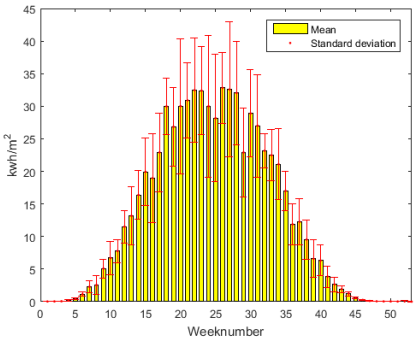


**(a)** Solar measurement, the yellow bars are the mean for each week and the red lines are the standard deviation

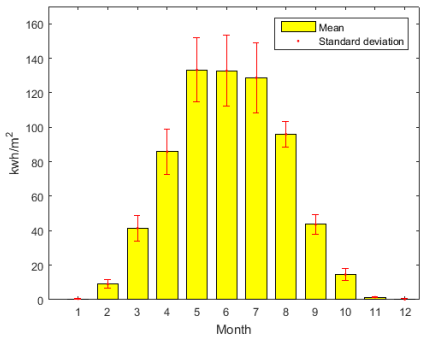


**(b)** Solar measurement, the yellow bars are the mean for each month and the red lines are the standard deviation

**Figure 4.22:** weekly and monthly solar measurements from Holt

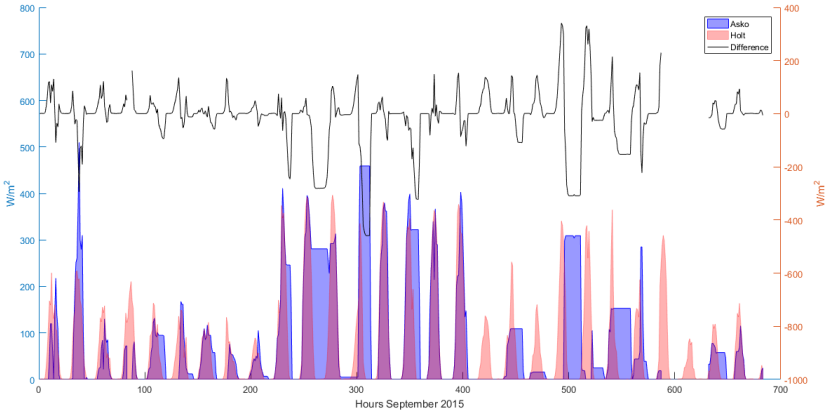


**Figure 4.23:** The solar measurement for most of September 2015. The red filled area is the measurement from Holt. The blue filled area is the measurement from Asko and the black line is the difference between them. The holes in the black line is from missing Asko data.

### 4.5.2 Energy output from solar panels

#### Horizontal surface

The mean irradiation from Holt, as shown in figure 4.21, is used to calculate the theoretical energy produced from a solar panel. In section 3.6.2 the efficiency of a Benq solar SunForte 327W was found to be $n_{STC} = 0.201$ and temperature dependent according to the theory in section 2.2.3. With that considered, the energy of a solar cell for one year is 144.3 $kWh/m^2$ without losses from inverter, cables etc. and assuming the given efficiency is correct.

### 4.5.3 Orientation and tilt

The energy from an orientated and tilted surface is dependent on more than the efficiency and temperature. The sun's orientation and elevation compared to the orientation and tilt of the solar cell is affecting the direct part of irradiation. As discussed in section 3.6.2 the direct is set to 75 % when the sun is not shadowed. The energy from the direct part is calculated from equation (2.2.14) and summed up with the energy from diffuse irradiation. The total energy is calculated with different orientation and tilt and shown in figure 4.24. Figure 4.25 shows the 26 configurations with yearly energy over 190 $kWh/m^2$. The maximum is when the orientation is 182° and the tilt is 47° with a yearly total of 193.13 $kWh/m^2$.

### 4.5.4 Two-axis tracking

The energy from two-axis tracking is calculated in a similar way as the orientated and tilted surface. The exception is that the energy from direct irradiation is calculated with (2.2.16) before summed up with the energy from the diffuse irradiation.

### 4.5.5 Summary of energy on solar cells

From week one to eight and 42 to 52 the weekly energy output is small and equal for all three types. This is during the winter when the is no sun or the sun is behind the mountains, all of the radiation is diffused/reflected. When passing week nine the sun is above the horizon, but low, making the horizontal solar cells little productive while the two other is able to utilize the direct radiation. In the summer, the horizontal produces almost the same amount as the orientated and tilted while the tracking produce a significant amount more. The orientated and tilted is facing south. In the night, the sun will be north of

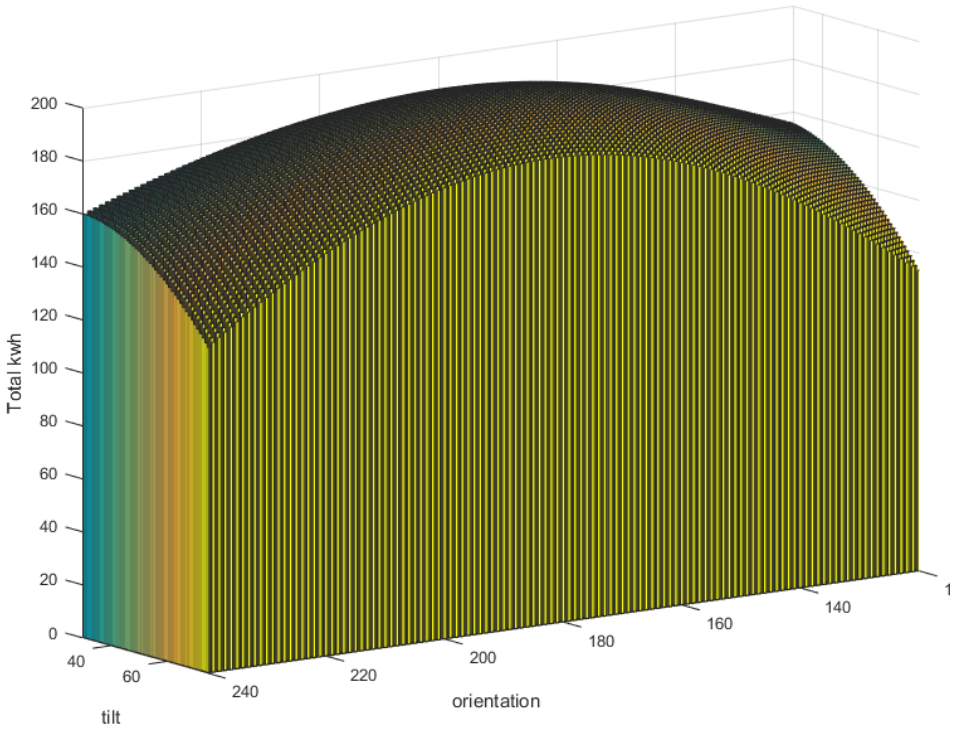


**Figure 4.24:** The total energy with different orientation and tilt

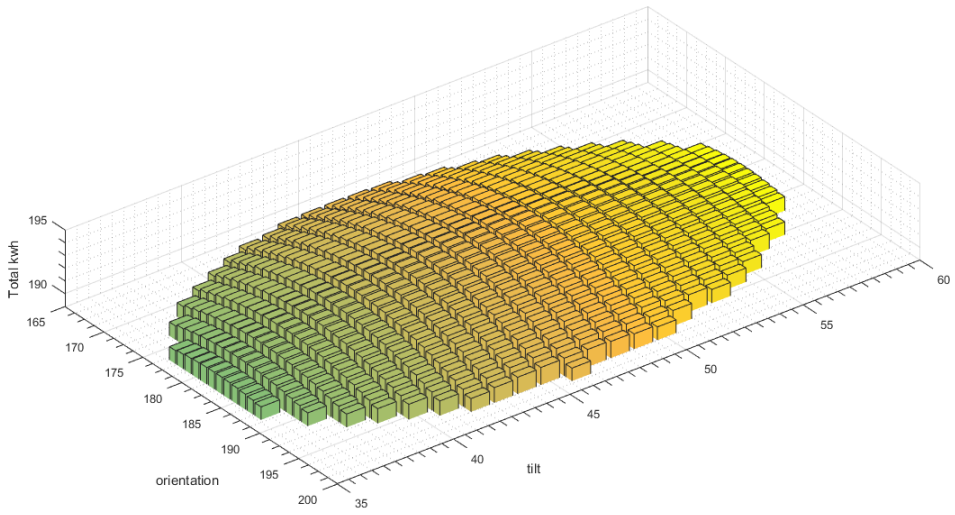


**Figure 4.25:** The orientation and tilt with energy over 190 $kWh/m^2$

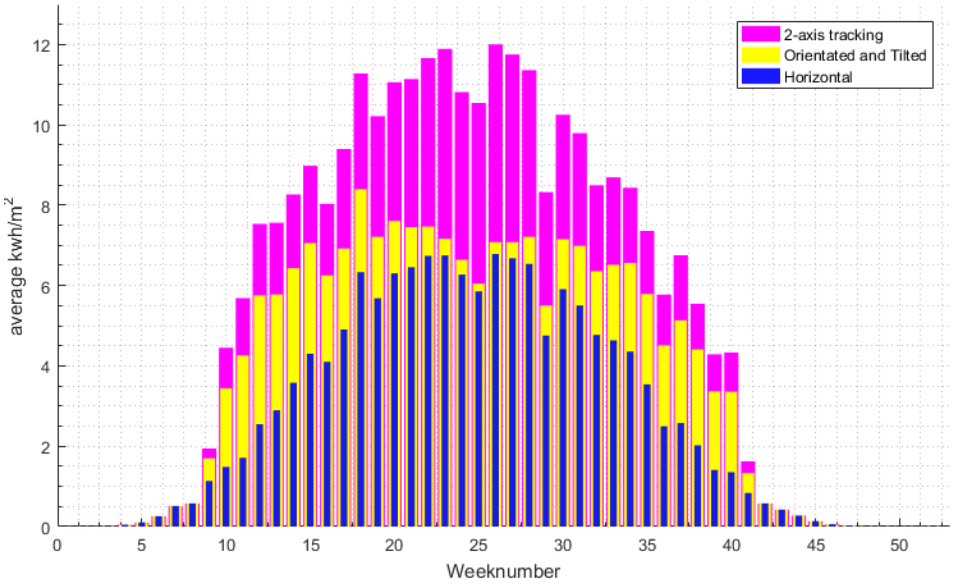


**Figure 4.26:** The bars are the energy output for each week for solar panel: Horizontal, Orientated and Tilted and with two-axis system

| Type \ Week | 1-9 | 10-19 | 20-29 | 30-39 | 40-49 | 50-53 | sum |
|---|---|---|---|---|---|---|---|
| Horizontal | 2.7 | 37.6 | 63.1 | 37.2 | 3.7 | 0.0 | 144.3 |
| $Y = 182°, \beta = 47$ | 3.2 | 61.6 | 69.3 | 56.8 | 6.2 | 0.0 | 197.1 |
| Tracking | 3.5 | 81.4 | 110.6 | 75.4 | 7.5 | 0.0 | 278.4 |

**Table 4.2:** The energy produced from the different types of solar cells at different weeks in $kWh/m^2$ without losses from inverter, cable etc., and a efficiency $n_{STC} = 0.201$

the panels and they will produce only a small amount of energy. In appendix A, the sun's motion on the 15th of every month is shown.

Orientating and tilting the solar panels will give an increase of 35.5 % and with tracking it will give an increase of 92.9 %. The energy used to track and move the solar panel is not considered here.

It is important to notice that all of these values are for a square meter of solar cell. In a real case, a panel does not cover the entire area, making the solar panel efficiency lower. Losses from inverter, cables etc. need to be considered.

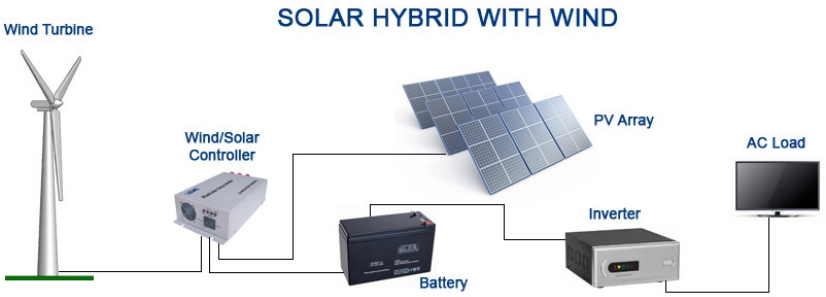


**Figure 4.27:** Example of solar hybrid wind system. Illustration by Energis smart energy solution [37]

## 4.6 Energy production example

To understand the amount of electricity Asko is able to produce, more factors are needed. Therefore, an example is made. The production from solar and wind is first calculated separately. Then the total production is compared with the usage. An overview of a solar and wind system is illustrated in figure 4.27.

### 4.6.1 The energy usage at Asko

The energy usage from the electrical grid was 3118151 kWh in 2014. Figure 4.28 shows the usage of energy each week. The red line is the average temperature each week. The green line is the calculated mean usage and have value $E_{mean}$ = 59964kWh. The week with lowest usage is week 16 with $E_{16}$ = 48795kWh or 18.73% less than the mean. The week with highest usage is week 50 with $E_{50}$ = 72438kWh or 20.81% more than the mean. These are the peaks, and all over the changes from week to week are not large. There are different temperature needs in the building. Some require cooling, some freezing and some room temperature. In normal houses, the energy usage is strongly dependent on temperature, where usage is high when outside temperature is low. The temperature in week 16, when the usage was lowest, was $T_{16} = 2.47°C$. $2.47°C$ is not far from the mean temperature. In the figure, a peak in both usage and temperature is shown from week 25 to week 30. This might suggest that under warmer days more energy is needed to hold the temperature down in the cooling and freezing area. Likewise, when the temperature is low over time, like week 43 to week 53, the usage rise over average.

Figure 4.29 shows the mean usage each hour of the day from one week in October 2015. This shows that between 06.00 and 07.00 in the morning the

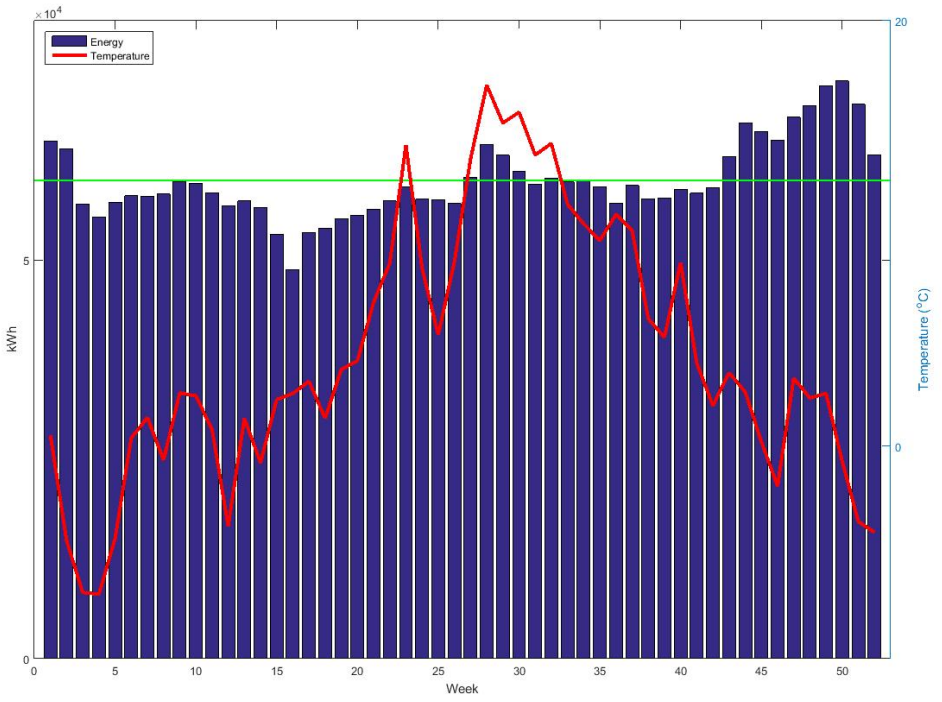


**Figure 4.28:** Electrical consumption each week in 2014 in blue, the average usage in green and temperature in red

usage is rising rapidly and stays high until 17.00, when it slowly decreases throughout the evening to 150 kwh each hour. This shows that there is a basis energy usage that is needed any time of the day even when there is no activity in the building. It should be noted that the plot is only based on seven days and two of them was in a weekend.

### 4.6.2 Solar

The roof of Asko is large and without limitations it would have been a great location. Unfortunately, the roof is only constructed to handle 650 $kg/m^2$. This is a problem during winter when snow is on the roof. The solar panels can no be in conflict with removing the snow. And the extra weight of the solar panels does not make it better. The Benq solar SunForte 327W solar panel module is 1559x1046$mm$ and weigh 18.6 $kg$ without the mounting [39]. At tilted 47°, the weight is spread out on 1.617 $m^2$ giving 15.8 $kg/m^2$ without the mounting. The mounting is not expected to be too heavy. Hence, in this case, the weight of the solar panels is not taken into account, only the

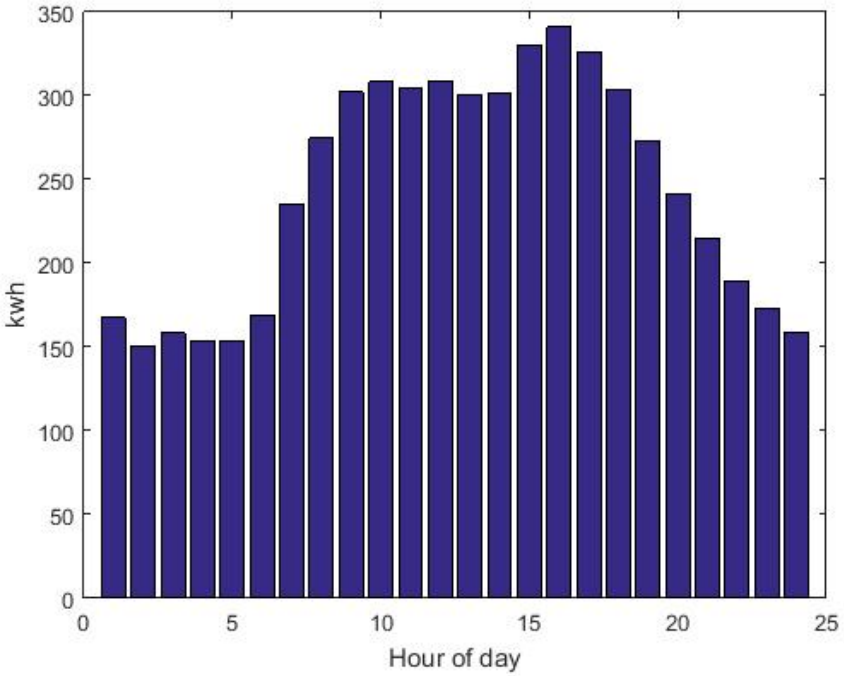


**Figure 4.29:** Electrical consumption based on hour of day

removal of snow. Figure 4.31 show three rows of solar panels as an option. The blue rows are solar panels with optimal tilt and orientations. The red line is panels mounted vertical. Since snow removal is necessary, the green arrows could be a solution to the removal of the snow. Row one is 103 meters and row two is 183 meters. Both rows will have three modules next to each other with the long sides down according to figure 4.30. This is to minimize losses when snow covers the lower parts of the module. With this configuration, row one will have 180 modules, leaving 10 m free, and row two will 330 have modules, leaving 12 m free, each 1.63 $m^2$. Together that equals 831 $m^2$ of solar modules. Row three will be mounted straight on the wall. The wall is pointing at 140°. As discussed in section 4.5.3 this is not optimal for production. However, it is optimal for the building. The wall is 80 meters long and 9.5 meters high. This gives room for three modules in height and 75 in the length with the modules standing with the long sides upwards. That equals 733$m^2$ of solar panels.

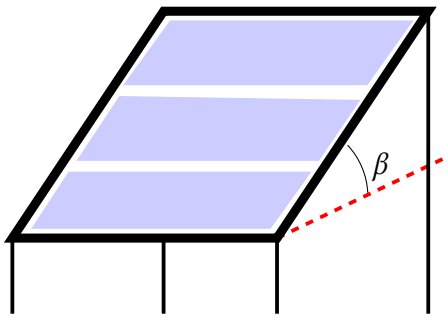


**Figure 4.30:** Three solar modules next to each other

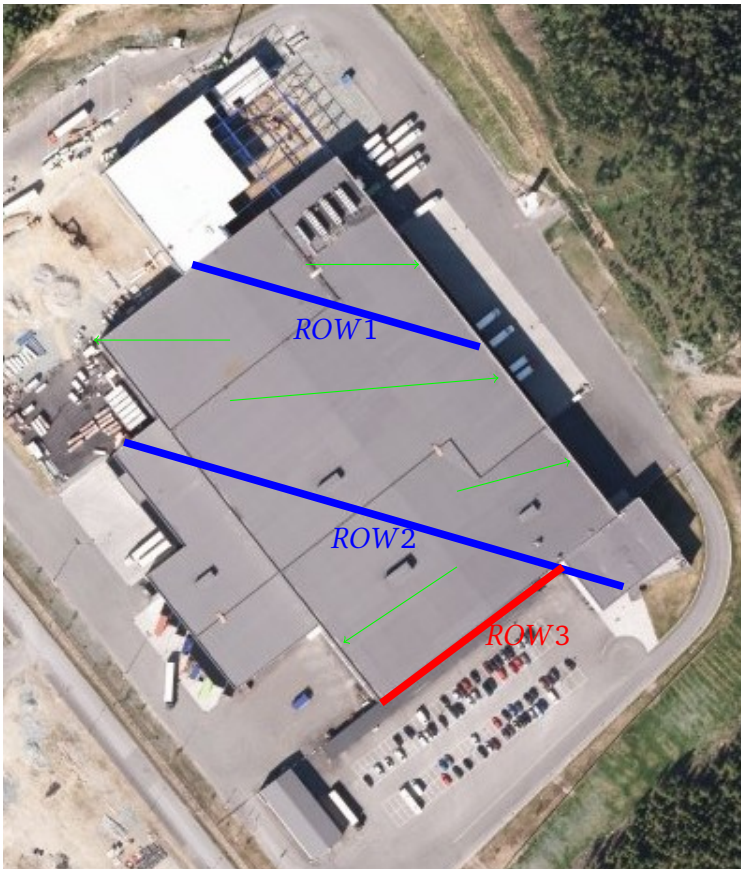


**Figure 4.31:** Aerial photo over Asko's area with placement of three rows with solar panels. Photo from kartverket.no

| Type | Without losses | With losses | $kWh/kW_p$ |
|---|---|---|---|
| Horizontal | 144.3 $\frac{kWh}{m^2y}$ | 121.2 $\frac{kWh}{m^2y}$ | 604.2 |
| $Y = 182°, \beta = 47$ | 197.1 $\frac{kWh}{m^2y}$ | 165.6 $\frac{kWh}{m^2y}$ | 825.3 |
| $Y = 140°, \beta = 0$ | 143.8 $\frac{kWh}{m^2y}$ | 120.8 $\frac{kWh}{m^2y}$ | 602.1 |
| Tracking | 278.4 $\frac{kWh}{m^2y}$ | 233.9 $\frac{kWh}{m^2y}$ | 1165.7 |

**Table 4.3:** The Energy produced produced with a Benq solar SunForte 327W module with $n_{STC} = 0.201$ and $W_p = 327W$

The values in figure 4.26 and table 4.2 are without losses from inverters etc. The performance ratio (PR) is the ratio of energy from solar panels that is converted to electricity. Reich et al. [34] tested the PR on 100 solar system in Germany. The systems have a mean PR of 84 %. The mean value is used for the Asko system.

The electricity produced from row one and row two will be 137613 $kWh$ each year and row three will have a production of 88546 $kWh$ each year. If the total usage was to be produced from solar it will need 18834 $m^2$ or 11554 solar modules with optimal orientation and tilt, or 13334 $m^2$ or 8181 solar modules with tracking.

### 4.6.3 Wind

The average wind is far from optimal. The measured and all the increased averages is under 3 $m/s$. Therefore, it is even more important to use the knowledge to choose correct locations. It is shown that the wind mainly comes from two directions, east and west. Therefore, the behaviour of wind from this direction is mainly considered.

It is demonstrated that turbulence will be an issue. Some figures show that at above twice the height of the building the majority of turbulence will be gone. However, this is not exact and not illustrated for all wind directions. There will probably be turbulence over the limit.

In the theory section, different types of wind turbines is discussed. One advantage of VAWT, compared to HAWT, is production in turbulent air. The VAWT also have lower rotational speed and noise. Noise is important when integrating the turbine in urban areas where people work. Table 2.2 also shows that

H-rotors have lower noise than both Darrieus and HAWT. H-rotors also have the possibility to be in a tower so it can be lifted to the proper height. In this case, a H-rotor is selected.

There are many manufactures of H-rotors. For this example the Aeolos 10 $kW$ H-rotor is chosen. The wind turbine has a low cut in wind speed of 2.5 $m/s$ and the rated wind speed is 12 $m/s$ and the cut-out wind speed is 55 $m/s$, the same as the survival wind speed. The weight of the turbine is 680 $kg$. There are two options, Place it away from the building or reinforce the roof. In this case, six wind turbines were to be installed, three close to the north-west wall and three close to the south-east wall on reinforced roof. The Aeolos have different tower heights. By choosing a 12 meter heigh tower, the wind turbine will be in the enhanced zone when it is above the wall facing the wind, and will avoid much of the turbulence when wind is from the opposite side. The example placement is shown in figure 4.32 where the yellow circles represent the wind turbines.

The energy from the six wind turbines is calculated with the corresponding power curve values and with wind measurement increased by 20 %. The yearly energy for each turbine will be 13166 $kWh$ and a total of 78996 $kWh$. To cover the total usage with wind turbines, Asko will need 237 Aeolos 10 $kW$ H-rotor wind turbines.

### 4.6.4 Total production compared to the usage

The electrical usage and the production is shown in figure 4.33. This shows that even in the weeks with the most energy production, Asko is not close to being self supplied. That said, this does not mean that it is a poor investment. The usage is large. Therefore, the production seems relatively small. Over the year the production is 305155 $kWh$, with a usage of 3118151 $kWh$, Asko is able to produce 9.8 % if the usage themselves. The figure shows that in this case, the energy production from solar is larger than the production from the wind. One weakness of this example are that the cost and energy prices in not considered. Therefore, it is hard to estimate which recourse gives the largest value even if solar have the biggest production.

## 4.7 Additional discussion

Many of the results have been discussed as they were presented. However, there are some issues that need to be further discussed.

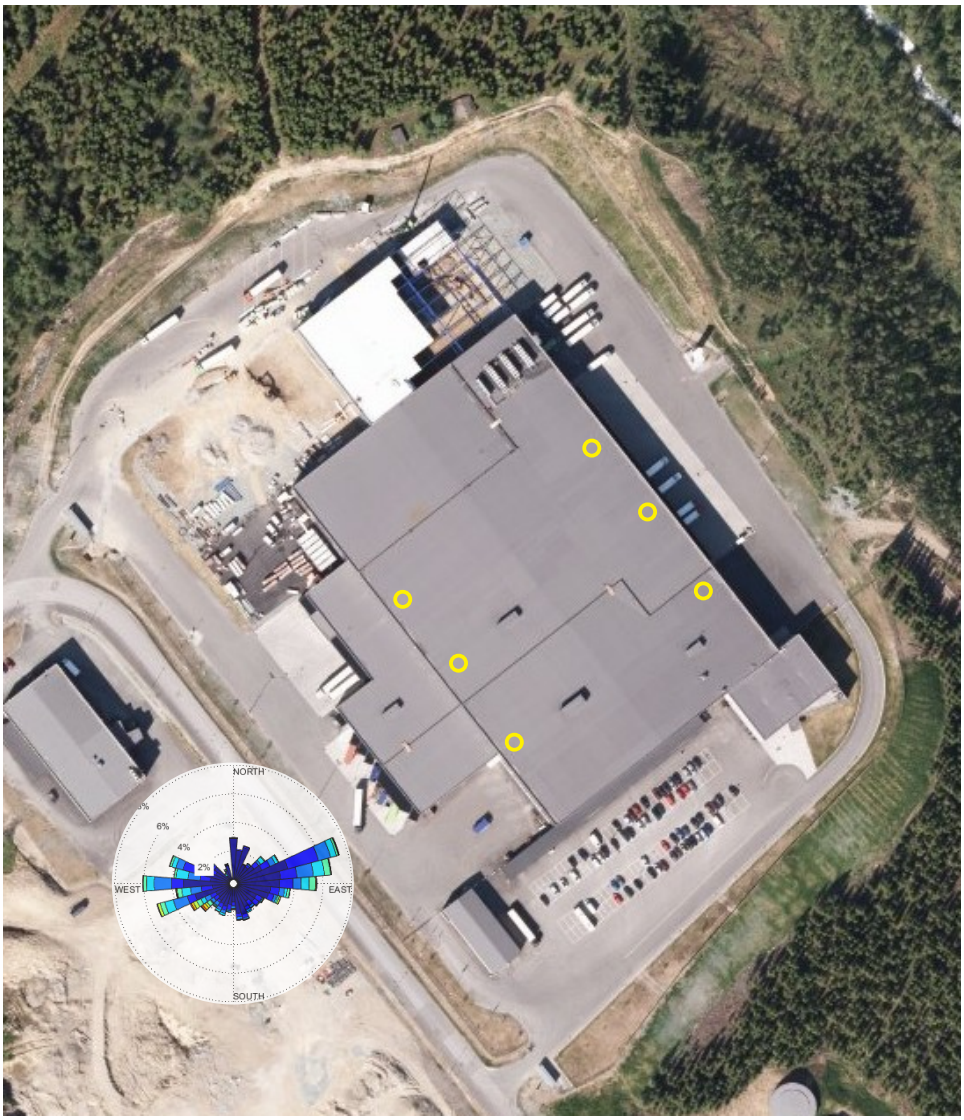


**Figure 4.32:** Example placement of wind six VAWT wind turbines.

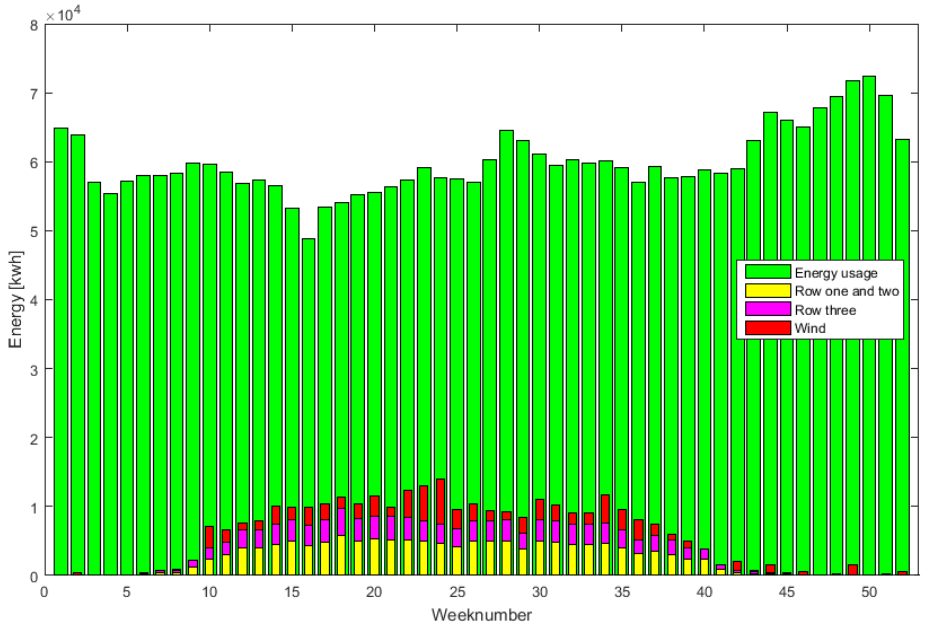


**Figure 4.33:** Production compared to usage at Asko

### 4.7.1 Limitations of Flow design

As mention in section 3.5.2 the input to the program is limited. The result is affected by this limitations. Boundary conditions are not an option, and neither is discussed in the information about the program. There is no option to change the wind speed with height into the tunnel. As discussed in section 2.1.4 and section 3.5.1 the wind is normally not constant in heights. The increase of measurement with 10%, 20% and 30% might not be enough when including placement of wind sensor, enhancement and wind share. An option is to use a set of wind speeds that change with time and measure specific points would give more accurate results.

### 4.7.2 Placement of wind sensor

It is already discussed that the wind sensor is not placed at a good location. There are more reasons for that. Multiple figures, for example figure 4.8, show that the wind measurement is in a belt of low wind from the edge of the roof. The most convenient location is often not a good choice and will lead to error.

# 5 Conclusion

## 5.1 Results

When considering wind, the result shows that there is an amount of useful energy in wind. However, as energy is in third factor of wind speed it is the dominant factor. measurement shows that the wind speeds are fairly low, , with a mean of 2.26$m/s$. By increasing the area of the wind turbine to compensate for low wind speeds, the wind turbine will be able to produce a significant amount of electricity. Then again, the cost increases with the size of the turbine. The second finding from the wind results is that the wind sensor is not placed at a good location. The sensor need to be at a greater distance above the roof to minimize turbulence and effects from the edges.

The solar results give a mean irradiation of 687.35 $kWh/m^2$ on a horizontal surface. This is lower than many other locations in the world. However, with temperature dependent efficiency and optimal orientation and tilt or tracing, there are good possibilities to produce electricity from solar irradiation. With that concluded, the optimal orientation and tilt for energy production is not always the best solution when building structure and limitations is considered. It is shown that solar panels mounted directly at a wall is a good usage of space and requires no structural change while still producing a significant amount of energy.

The main results show that Asko is able to set an example for other commercial businesses by producing energy for own use, even if only 9.8% of the usage is

covered. The produced energy is 100% renewable, making a positive effect on the climate both locally and globally.

## 5.2 Future work

The next step in a case like this is to make a cost/benefit analysis. The value have to be separated into an economical and environmental section. It would be interesting to look into the vehicle park and look at opportunities to use sustainable fuels or smart solutions to reduce the usage of fossil fuels. If the wind sensor is moved, it would be interesting to compare the new measurement with the present measurements and the results from wind simulation.

# Bibliography


[1] John David Anderson and J Wendt. *Computational fluid dynamics*, volume 206. Springer, 1995.

[2] John Andrews and Nicholas Alfred Jelley. *Energy Science: Principles, Technologies, and Impacts*. Oxford University Press, 2007.

[3] *Rev 01072014 Flow Design Preliminary Validation Brief*. Autodesk, 2016. URL `http://download.autodesk.com/us/flow_design/Flow_Design_Preliminary_Validation_Brief_01072014.pdf`. Accessed: 30.05.2016.

[4] Rebecca L Busby. *Wind Power: The Industry Grows Up*. PennWell Books, 2012.

[5] M.Z. Jacobson C.L. Archer. Wind energy. 2005.

[6] A Clifford Cohen. Maximum likelihood estimation in the weibull distribution based on complete and on censored samples. *Technometrics*, 7(4): 579–588, 1965.

[7] K Conradsen, LB Nielsen, and LP Prahm. Review of weibull statistics for estimation of wind speed distributions. *Journal of Climate and Applied Meteorology*, 23(8):1173–1183, 1984.

[8] *Davis Vantage pro 2 anemometer specification sheets*. Davis Instruments, 2016. URL `http://www.davisnet.com/support/anemometer/`. Accessed: 01.06.2016.

[9] *Davis Vantage pro 2 console manual*. Davis Instruments, 2016. URL `http://www.davisnet.com/product_documents/weather/spec_sheets/6152_62_53_63_SS.pdf`. Accessed: 01.06.2016.

[10] Bill Dunford and Katie McKissick. "solar system exploration: Planets: Sun: Facts and figures, 2016. URL `http://solarsystem.nasa.gov/planets/`

sun/facts. Accessed: 01.06.2016.

[11] Sandra Eriksson, Hans Bernhoff, and Mats Leijon. Evaluation of different turbine concepts for wind power. *Renewable and Sustainable Energy Reviews*, 12(5):1419–1434, 2008.

[12] D.L Evans. Simplified method for predicting photovoltaic array output. *Solar Energy*, 1981.

[13] BP global. Bp statistical review of world energy june 2015. 2015.

[14] Amelie Henden. Målt og modellert globalstråling ved ekofisk og i nordområdene. 2011.

[15] Christiana Honsberg and Stuart Bowden. Pve education, 2015. URL http://pveducation.org/pvcdrom.

[16] M Iqbal. An introduction to solar radiation. 1983.

[17] Morten Jacobsen. Short-term wind power prediction based on markov chain and numerical weather prediction models: A case study of fakken wind farm. Master's thesis, UiT The Artic University of Norway, 2014.

[18] Peter Jamieson. Hawt or vawt? *Innovation in Wind Turbine Design*, pages 211–222.

[19] Kaidor. Global circulation of earth's atmosphere displaying hadley cell, ferrell cell and polar cell, 2013. URL https://commons.wikimedia.org/wiki/File:Earth_Global_Circulation_-_en.svg. Accessed: 01.06.2016.

[20] Martin Kaltschmitt, Wolfgang Streicher, and Andreas Wiese. *Renewable energy: technology, economics and environment*. Springer Science & Business Media, 2007.

[21] *CM 11 pyranometer instruction manual*. Kipp & Zonen. URL http://www.kippzonen.com/Search.aspx?id=304&query=cm11#gsc.tab=0&gsc.q=cm11&gsc.page=1. Accessed: 01.06.2016.

[22] KoeppiK. This picture shows a wind turbine with an observation deck. the wind turbine is part of the wind park bruck an der leitha in lower austria, 2012. URL https://commons.wikimedia.org/wiki/File:Wind_turbine_with_observation_deck_bruck_an_der_leitha.jpg. Accessed: 01.06.2016.

[23] L Ledo, PB Kosasih, and P Cooper. Roof mounting site analysis for micro-wind turbines. *Renewable Energy*, 36(5):1379–1391, 2011.

[24] David Lingfors. Solar variability assessment and grid integration: Methodology development and case studies. 2015.

[25] ED Mehleri, PL Zervas, H Sarimveis, JA Palyvos, and NC Markatos. Determination of the optimal tilt angle and orientation for solar photovoltaic arrays. *Renewable Energy*, 35(11):2468–2475, 2010.

[26] Konstantinos Misiakos and Dimitris Tsamakis. Accurate measurements of the silicon intrinsic carrier density from 78 to 340 k. *Journal of applied physics*, 74(5):3293–3297, 1993.

[27] Jenny Nelson. *The physics of solar cells*, volume 1. World Scientific, 2003.

[28] Vaughn Nelson. *Wind energy: renewable energy and the environment*. CRC Press, 2009.

[29] BG Newman. Multiple actuator-disc theory for wind turbines. *Journal of Wind Engineering and Industrial Aerodynamics*, 24(3):215–225, 1986.

[30] Nibio. About agriculture meteorological service norway, 2016. URL `http://lmt.nibio.no/about`.

[31] Intergovernmental panel on climate change(IPPC). Summer for policimakers. 2014.

[32] K Pope, I Dincer, and GF Naterer. Energy and exergy efficiency comparison of horizontal and vertical axis wind turbines. *Renewable Energy*, 35(9): 2102–2113, 2010.

[33] Damian Pysch, Ansgar Mette, and Stefan W Glunz. A review and comparison of different methods to determine the series resistance of solar cells. *Solar Energy Materials and Solar Cells*, 91(18):1698–1706, 2007.

[34] Nils H Reich, Bjoern Mueller, Alfons Armbruster, Wilfried GJHM Sark, Klaus Kiefer, and Christian Reise. Performance ratio revisited: is pr> 90% realistic? *Progress in Photovoltaics: Research and Applications*, 20(6): 717–726, 2012.

[35] Peter J Schubel and Richard J Crossley. Wind turbine blade design. *Energies*, 5(9):3425–3449, 2012.

[36] JV Seguro and TW Lambert. Modern estimation of the parameters of the weibull wind speed distribution for wind energy analysis. *Journal of Wind Engineering and Industrial Aerodynamics*, 85(1):75–84, 2000.

[37] Energus smart energy solution. Solar hybrid with wind, 2016. URL http://energis.com.au/solar-wind-hybrid-systems/. Accessed: 01.06.2016.

[38] Chetan Singh Solanki. *Solar photovoltaics: fundamentals, technologies and applications*. PHI Learning Pvt. Ltd., 2011.

[39] Benq Solar. Sunforte pm096boo datasheet, 2016. URL http://www.benqsolar.com/?sn=1268&lang=en-US. Accessed: 01.06.2016.

[40] MF Stuckings and Andrew W Blakers. A study of shading and resistive loss from the fingers of encapsulated solar cells. *Solar energy materials and solar cells*, 59(3):233–242, 1999.

[41] TheNoise. p-n junction, 2007. URL https://commons.wikimedia.org/wiki/File:Earth_Global_Circulation_-_en.svg. Accessed: 01.06.2016.

[42] Francisco Toja-Silva, Antonio Colmenar-Santos, and Manuel Castro-Gil. Urban wind energy exploitation systems: Behaviour under multidirectional flow conditions—opportunities and challenges. *Renewable and Sustainable Energy Reviews*, 24:364–378, 2013.

[43] Geoffrey K Vallis. *Atmospheric and oceanic fluid dynamics: fundamentals and large-scale circulation*. Cambridge University Press, 2014.

[44] W.Wacker. Darriues wind power generator near heroldstatt, germany, 2005. URL https://commons.wikimedia.org/wiki/File:Darrieus_rotor001.jpg. Accessed: 01.06.2016.

# Appendix:

# A

# Solar movement for the 15th of each month

January

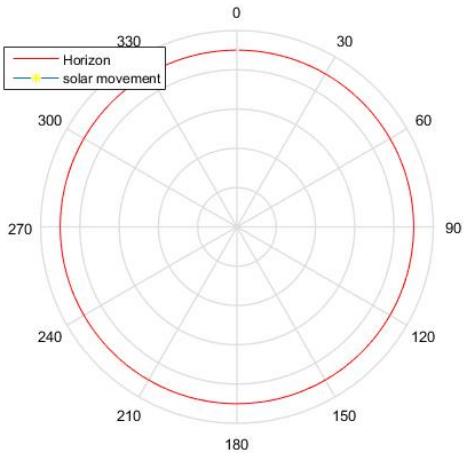


February

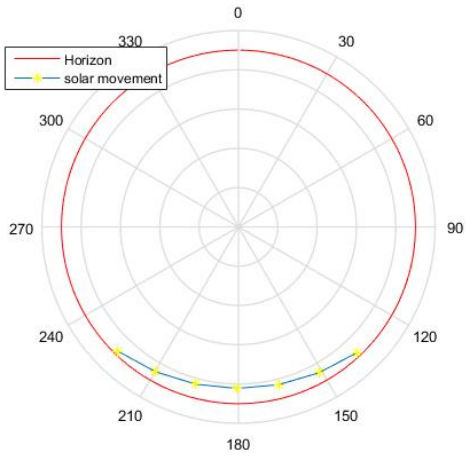


Mars

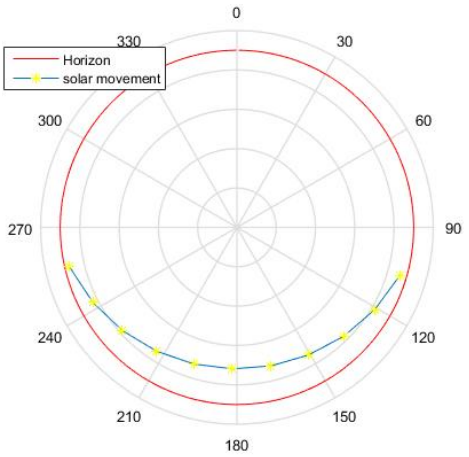


April

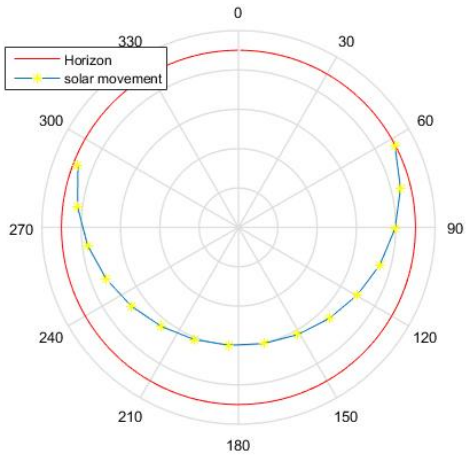


May

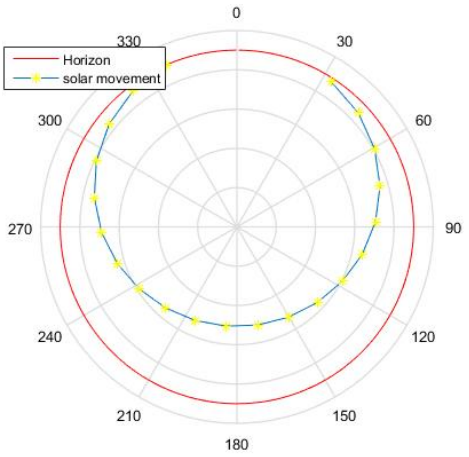


June

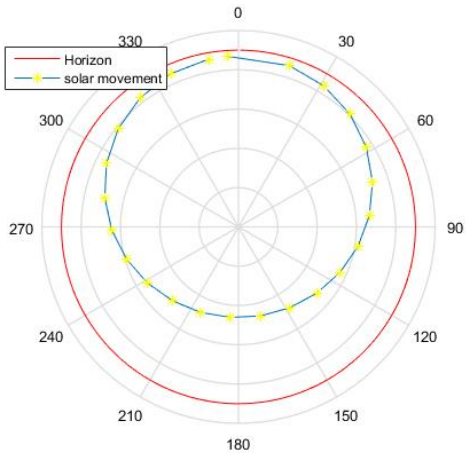

July

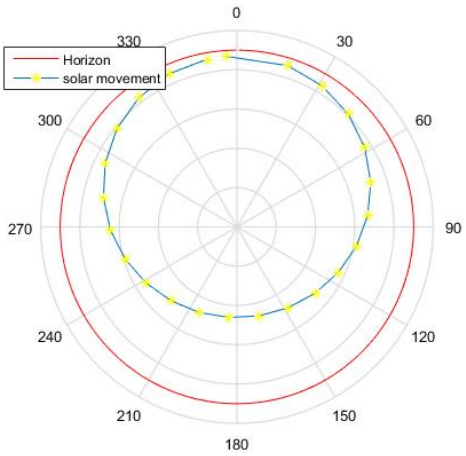


August

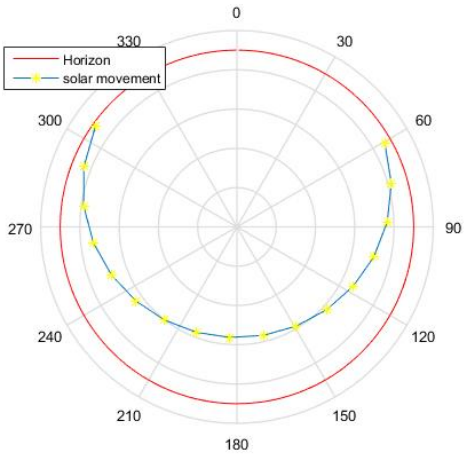


September

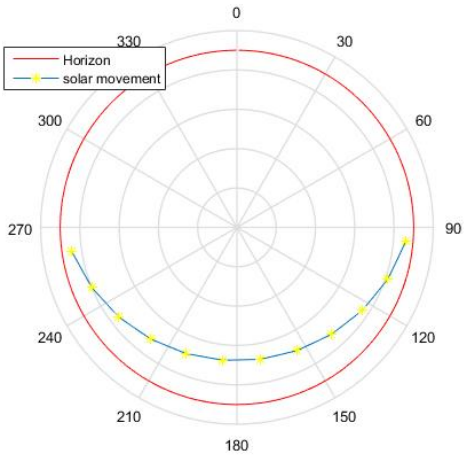


October

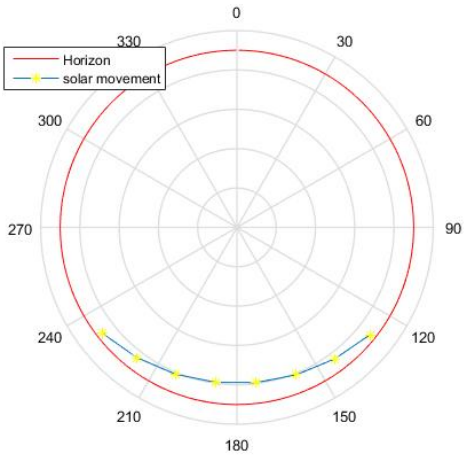


November

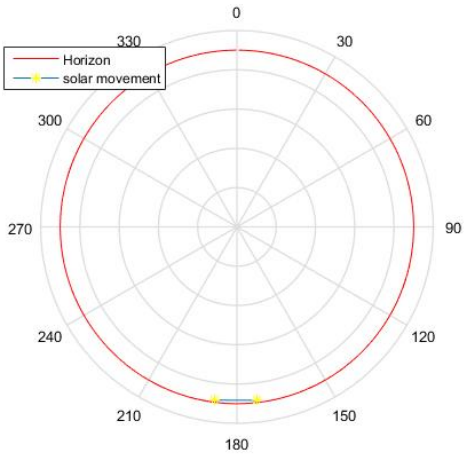


December

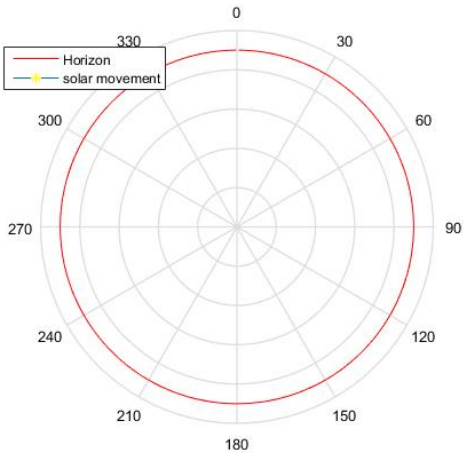

# B

# Periodic table of the elements

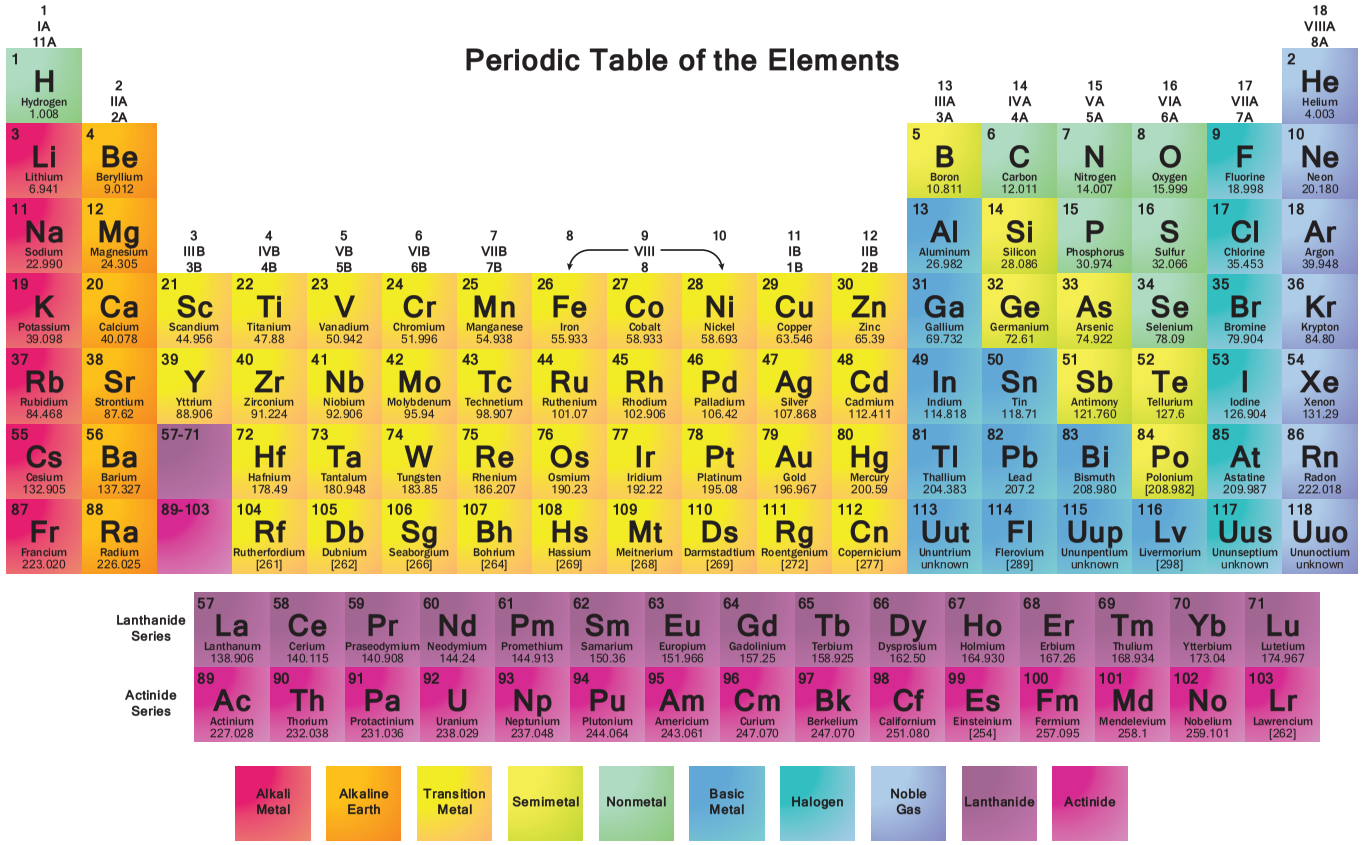


Figure from Todd Helmenstine, 2013